symmetry

MDPI

Article

A Mathematical Model of Dengue and Lassa Fever Co-Infection with Education and Vector Control

Kefas Bitrus [1,2], Farah Aini Abdullah [2,3,*], Matthew O. Adewole [2,4], James Andrawus [5], Sania Qureshi [6,7], Amanullah Soomro [6], Samuel Adamu [8], Idris Ahmed [9], Rakiya Mohammed Ngoshe [10] and Chanakarn Kiataramkul [11,*]

1 Department of Mathematics, Federal University Lokoja, Lokoja 1154, Kogi State, Nigeria; kefas.bitrus@fulokaja.edu.ng
2 School of Mathematical Sciences, Universiti Sains Malaysia, Gelugor 11800 USM, Pulau Pinang, Malaysia; olamatthews@ymail.com
3 Nonlinear Dynamics Research Center (NDRC), Ajman University, Ajman, P.O. Box 346, United Arab Emirates
4 Mathematics Programme, Bowen University, Iwo P.M.B. 284, Osun State, Nigeria
5 Department of Mathematics, Federal University Dutse, Dutse 7156, Jigawa State, Nigeria; james.a@fud.edu.ng
6 Department of Basic Sciences and Related Studies, Mehran University of Engineering & Technology, Jamshoro 76062, Pakistan; sania.qureshi@faculty.muet.edu.pk (S.Q.); amanullah.soomro@faculty.muet.edu.pk (A.S.)
7 Research Center of Applied Mathematics, Khazar University, Baku 1009, Azerbaijan
8 Department of Mathematics, Nigeria Army University Biu, Biu 1500, Borno State, Nigeria; samuel.adamu@naub.edu.ng
9 Department of Mathematics, Faculty of Natural and Applied Sciences, Sule Lamido University Kafin Hausa, Kafin Hausa P.M.B. 048, Jigawa State, Nigeria; idris.ahmed@slu.edu.ng
10 Department of Medicine, Nile University of Nigeria, Abuja 900001, Nigeria; rakiya.ngoshe@nileuniversity.edu.ng
11 Intelligent and Nonlinear Dynamic Innovations Research Center, Department of Mathematics, Faculty of Applied Science, King Mongkut's University of Technology North Bangkok, Bangkok 10800, Thailand
* Correspondence: farahaini@usm.my (F.A.A.); chanakarn.k@sci.kmutnb.ac.th (C.K.)

Abstract

Dengue and Lassa fever co-circulate in Nigeria, yet few models examine their co-infection alongside behavioural and clinical interventions. This study develops a deterministic compartmental model of dengue–Lassa fever co-infection that couples human, mosquito and rodent dynamics and distinguishes educated from uneducated susceptible individuals. We derive the basic and effective reproduction numbers using the next-generation operator approach, and establish local and global stability of the disease-free equilibrium via a Lyapunov function, together with global stability of the endemic equilibria using a Goh–Volterra function. Sensitivity analysis identifies the parameters that most strongly influence transmission, and the model is calibrated against Nigerian surveillance data. Numerical simulations confirm the analytical results and show that public education, reduced human–vector contact and treatment of co-infected cases lower infection levels.

Keywords: co-infection; vectors; reproduction number; rodent; *Aedes aegypti*; *Mastomys natalensis*

Check for updates

Academic Editor: Linjie Liu

Received: 23 September 2026
Revised: 27 October 2026
Accepted: 10 November 2026
Published: 17 November 2026

Copyright: © 2026 by the authors. Licensee MDPI, Basel, Switzerland. This article is an open access article distributed under the terms and conditions of the Creative Commons Attribution (CC BY) license.

1. Introduction

Lassa hemorrhagic fever is a severe form of Lassa fever, a zoonotic viral illness caused by the Lassa virus [1–4]. The multimammate rat (*Mastomys natalensis*) is the virus host. Direct or indirect contact with food or objects contaminated with the urine or faeces of sick multimammate rats is the main way the disease spreads from these rats to humans [5]. Other possible routes of infection include rodent-to-rodent and person-to-person transfer. Lassa

fever was first identified in 1969 in Borno State, Nigeria, near the settlement of Lassa [6,7]. Since then, numerous mathematical models have been developed to tackle the issue [5,7]. A single case of dengue and Lassa virus co-infection has been documented in Oyo State, Nigeria [8].

Tropical and subtropical areas worldwide are home to dengue, a virus spread by mosquitoes [9–12]. In the ten years that followed its designation in 1779, the disease's earliest documented epidemics happened concurrently on three continents: Asia, Africa and North America [13]. Recently, Bitrus et al. [8] emphasized the need for public awareness and the role it plays in controlling dengue fever. Lassa fever has an incubation period of six to twenty-one days [14], in contrast to several other infectious diseases described in [15–20]. Another study reports that Lassa fever usually incubates for 1 to 3 weeks, or from the moment of exposure to the Lassa virus until symptoms appear [7,21]. Currently, no vaccine against Lassa fever is available; consequently, reducing disease spread between individuals depends heavily on infection control strategies. Eliminating the rodent population is not a feasible solution.

Types 1 and 2 of the dengue virus have long been known to cause dengue haemorrhagic fever in Nigeria and other tropical countries [19,22,23]. Seroepidemiological surveys indicate high dengue virus activity in the country; however, knowledge of dengue and haemorrhagic fever remains limited. This is mainly because dengue fever presents as classical dengue fever, which is characterized by fever, myalgia, headache, arthralgia, retro-orbital pain, gastrointestinal symptoms and skin rash [22]. Between 1964 and 1968, dengue viruses (DENVs) were initially isolated from febrile patients seen at the outpatient clinic of University College Hospital, Ibadan, Nigeria [14,19,22]. The insecticidal properties of a few chosen ethnobotanicals against culicine mosquitoes in an effort to control vectors were examined by [24] and it was discovered that the results were successful. Two strategies to stop dengue and Lassa fever from spreading, which are the aims of this study, are: promoting good hygiene habits at home to avoid contact with waste products from infected rats, and setting up well-equipped medical facilities for efficient patient screening, diagnosis and treatment.

Mathematical modelling has been widely used to examine the transmission dynamics of both diseases. For dengue, models have explored vaccination [2,12], vector control [23] and the role of public awareness [8]. For Lassa fever, models have focused on rodent-to-human transmission, environmental contamination and treatment [1,3,5,7,21]. Co-infection models combining dengue with other pathogens exist, but they typically address dengue–leptospirosis or dengue–tuberculosis co-infection rather than dengue–Lassa fever.

A separate line of work has replaced the integer-order derivative by a fractional operator, which introduces a memory trace that decays as the order approaches unity. Models of this kind have been developed for psoriasis with drug treatment [25,26], for tumour cell dynamics [27], and for measles with Reye's syndrome fitted to UK surveillance data [28]. The present model is integer-order throughout; we mention this literature because extending the model to fractional order, in which the current state depends on the history of the epidemic rather than on its instantaneous value, is a natural direction for future work.

A parallel line of work has examined mosquito suppression directly, rather than through the epidemiology of the diseases they transmit. Fawzy et al. [29] formulated a Filippov model in which sterile mosquitoes are released only when the wild population exceeds a threshold, and showed that the resulting dynamics include sliding bifurcations, bistability and hysteresis, with the practical conclusion that a lower threshold improves control while reducing cost. The same group extended this framework to the incompatible insect technique [30]. These studies treat the mosquito population as the dynamical system of interest and do not couple it to human infection dynamics. The present model takes the complementary approach: it represents vector control through its effect on the mosquito

mortality rate μ_v, and asks how that effect propagates to the reproduction number and to the infected human compartments. The two perspectives are therefore complementary, and combining them is a natural direction for future work.

Several mathematical models have examined dengue and Lassa fever separately, and a few have considered co-infection with other pathogens. However, existing studies have not, to our knowledge, simultaneously incorporated educated and uneducated susceptible classes, coupled mosquito and rodent vector dynamics, and treatment of co-infected individuals within a single framework. The model proposed here therefore extends the literature in three respects: it represents the transition of susceptible individuals from an uneducated to an educated class, it couples two distinct vector–host transmission pathways, and it allows for the clinical management of co-infected cases. These features distinguish the present work from earlier dengue models, including those of [31,32], which focus on single-disease dynamics without the co-infection and education structure considered here.

2. Model Formulation

We developed a deterministic mathematical model for the transmission dynamics of Dengue and Lassa fever co-infection considering education on vector control as a vital tool to control such a plague. The human population is divided into nine compartments: uneducated susceptible S_u, educated susceptible S_e, exposed to dengue E_d, exposed to Lassa fever E_l, dengue infectious I_d, Lassa fever infectious I_l, dengue–Lassa fever co-infectious I_{dl}, co-infection treatment T_{dl}, and recovered R. The mosquito population is divided into susceptible S_v and infectious I_v classes, and the rodent population into susceptible S_r and infectious I_r classes. The susceptible become infected by frequent exposure to Infected Aedes aegypti species of mosquitoes and by direct or indirect exposure to food or other items contaminated with urine or feces of infected multimammate rats (Mastomys natalensis) at a rate λ_d or λ_l respectively known as the mass-exposure action.

Vector control is represented by two parameters: the mosquito mortality rate μ_v, which is increased by measures such as the use of repellents and the removal of breeding sites, and the rodent mortality rate μ_r, which is increased by rodent control measures. Thus, ϕ is defined as $\phi_1 = (1 - t_1)$ and $\phi_2 = (1 - t_2)$ where $0 \leq t_1, t_2 \leq 1$ is the viability of the control measure taken by an individual depending on compliance. If $t_1, t_2 = 1$, then the control provides maximum protection against dengue and Lassa fever infection; on the other hand, if $t_1, t_2 = 0$, then the control was not applied. When $0 < t_1 < t_2 < 1$, the control is more effective against dengue than against Lassa fever, so that an educated susceptible individual is infected at a lower rate by dengue than by Lassa fever. If further $t_1 = 0$ and $t_2 = 1$, it means the control worked for Dengue fever but failed for Lassa fever infection. Similarly, if $t_1 = 1$ and $t_2 = 0$, the control worked for Lassa fever infection but failed for dengue fever; these cases are examined in the subsequent Section. In this paper we base our idea on the work of [20], who studied the co-infection of a zoonotic bacterial disease called leptospirosis, which is one of the most significant neglected tropical bacterial diseases and one of the leading zoonotic causes of morbidity in the world, and dengue fever. In their work, they highlighted several similarities between dengue fever and leptospirosis, as well as methods of controlling some mammals that cause the diseases. This study specifically addresses the co-infection dynamics of dengue and Lassa fever, a pressing health concern in Nigeria, while emphasizing education on novel vector management methods as an intervention tool. Thus, the co-infection model is given in Figure 1, where description of the state variable is given in Table 1 and consists of the following set of variables:

$$\{S_u(t); S_e(t); E_d(t); E_l(t); I_d(t); I_l(t); I_{dl}(t); T_{dl}(t); R(t)\},$$

$$\{S_v(t); S_r(t); I_v(t); I_r(t)\}.$$

Human population:

$$\begin{aligned} N_h =& S_u(t) + S_e(t) + E_d(t) + E_l(t) + I_d(t) + I_l(t) \\ &+ I_{dl}(t) + T_{dl}(t) + R(t). \end{aligned} \tag{1}$$

Vector population—mosquito species (*Aedes aegypti*):

$$N_v = S_v(t) + I_v(t). \tag{2}$$

Vector population—Rodent, the multimammate rat (*Mastomys natalensis*):

$$N_r = S_r(t) + I_r(t). \tag{3}$$

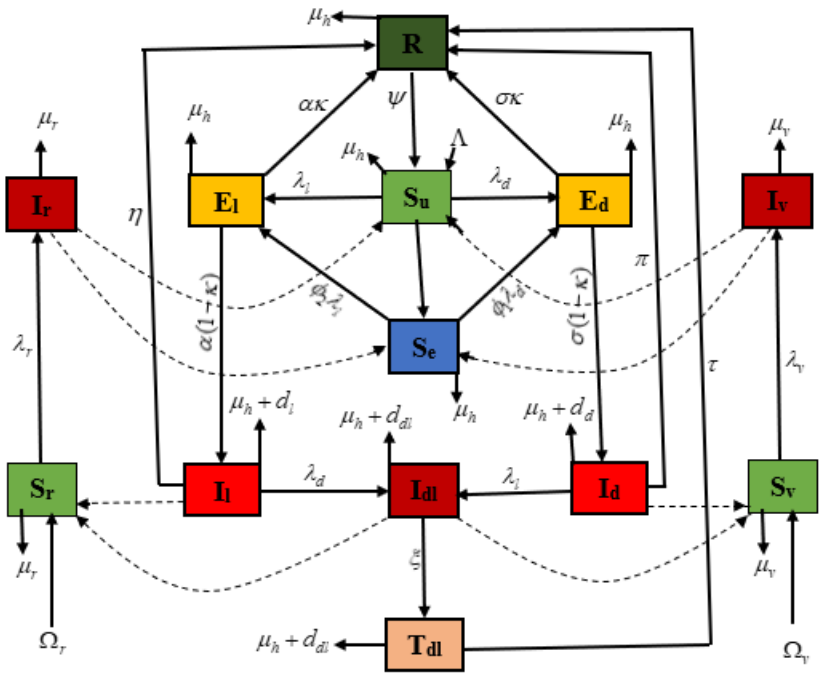


Figure 1. Schematic diagram of dengue–Lassa fever co-infection.

Table 1. Interpretation of the state variables used in the model (4).

Variable	Description
N_h, N_v, N_r	Total population of humans, vectors and rodents
S_u, S_e	Uneducated and educated Susceptible humans
E_d, E_l	Exposed Dengue and Lassa fever individuals
I_d, I_l	Infectious Dengue and Lassa fever individuals
I_{dl}	Co-infectious individuals
T_{dl}	Co-infectious individuals under Treatment
R	Recovered individuals
S_v, S_r	Susceptible vectors and rodents
I_v, I_r	Infectious vectors and rodents

$$
\begin{aligned}
\frac{dS_u}{dt} &= \Lambda + \psi R - (\lambda_d + \lambda_l + \epsilon + \mu_h)S_u, \\
\frac{dS_e}{dt} &= \epsilon S_u - (\phi_1\lambda_d + \phi_2\lambda_l + \mu_h)S_e, \\
\frac{dE_d}{dt} &= \lambda_d S_u + \phi_1\lambda_d S_e - (\sigma + \mu_h)E_d, \\
\frac{dI_d}{dt} &= (1-\kappa)\sigma E_d - (\pi + \lambda_l + \mu_h + d_d)I_d, \\
\frac{dS_v}{dt} &= \Omega_v - (\lambda_v + \mu_v)S_v, \\
\frac{dI_v}{dt} &= \lambda_v S_v - \mu_v I_v, \\
\frac{dE_l}{dt} &= \lambda_l S_u + \phi_2\lambda_l S_e - (\alpha + \mu_h)E_l, \\
\frac{dI_l}{dt} &= (1-\kappa)\alpha E_l - (\eta + \lambda_d + \mu_h + d_l)I_l, \\
\frac{dS_r}{dt} &= \Omega_r - (\lambda_r + \mu_r)S_r, \\
\frac{dI_r}{dt} &= \lambda_r S_r - \mu_r I_r, \\
\frac{dI_{dl}}{dt} &= \lambda_l I_d + \lambda_d I_l - (\xi + \mu_h + d_{dl})I_{dl}, \\
\frac{dT_{dl}}{dt} &= \xi I_{dl} - (\tau + \mu_h + d_{dl})T_{dl}, \\
\frac{dR}{dt} &= \sigma\kappa E_d + \alpha\kappa E_l + \tau T_{dl} + \pi I_d + \eta I_l - (\psi + \mu_h)R.
\end{aligned} \tag{4}
$$

where

$$
\lambda_d = \frac{\beta_{hd} I_v}{N_v}, \lambda_l = \frac{\beta_{hl} I_r}{N_r}, \tag{5}
$$

and

$$
\lambda_r = \frac{\beta_r I_l}{N_h}, \lambda_v = \frac{\beta_v I_d}{N_h} \tag{6}
$$

The model contains three treatment rates, π, η and ξ, which act on I_d, I_l and I_{dl}, respectively; Table 2 gives their precise definitions.

Table 2. Interpretation of parameters used in the model (4).

Parameter	Description
$\Lambda, \Omega_v, \Omega_r$	Recruitment rate of humans, vectors and rodents
ξ	Treatment rate of I_{dl}
μ_h, μ_r	Natural mortality rate of humans and rodents
μ_v	Natural mortality rate of vectors
ϵ	Education rate of uneducated susceptible humans
α	Progression rate of E_l to I_l
ϕ_1, ϕ_2	Control measure for Dengue and Lassa fever
σ	Progression rate of E_d to I_d
ψ	Rate at which R progress to S_u
τ	Recovery rate of I_{dl}
π	Recovery rate of infectious dengue fever I_d
d_d, d_l	Disease induced death rate of Dengue and Lassa fever
d_{dl}	Disease induced death rate of co-infected individuals
η	Recovery rate of infectious Lassa fever I_l
β_{hd}, β_{hl}	Effective contact rate of humans (Dengue), humans (Lassa)
β_v, β_r	Effective contact rate of vectors and rodents
κ	Proportion of E_d to R and E_l to R

The education rate ϵ should be interpreted as a summary of the net rate at which uneducated susceptible individuals become educated, rather than as a direct measure of any particular campaign. A campaign's effectiveness depends on its content, its reach, the duration of exposure to it, and whether the behaviour change is retained, and these factors are not represented separately in the model. The parameter ϵ therefore aggregates them into a single rate, and the simulations that vary ϵ should be read as exploring the consequences of different net rates of transition, not as predictions of the effect of any specific intervention.

The following assumptions are made in the formulation of the model.

1. First, dengue and Lassa fever exposures are modelled independently because the two pathogens have distinct transmission routes: dengue is transmitted by *Aedes aegypti* mosquitoes, whereas Lassa fever is transmitted primarily through contact with the excreta of *Mastomys natalensis*.
2. Second, co-infection is assumed to occur only when an individual is already infectious with one pathogen and is exposed to the other; this simplification avoids the combinatorial complexity of allowing co-exposure during the latent period and is consistent with the comparatively short incubation periods of both infections.
3. Third, recovered individuals from both infections are combined into a single compartment R because the model does not distinguish between pathogen-specific immunity.
4. Fourth, immunity following dengue, Lassa fever and co-infection is assumed to be identical and temporary, with individuals returning to the uneducated susceptible class at rate ψ; reinfection is therefore possible only after immunity has waned.
5. Fifth, dengue serotypes are not distinguished, so the model cannot capture serotype-specific interactions such as antibody-dependent enhancement.
6. Sixth, human-to-human transmission of Lassa fever is omitted because it is believed to be rare relative to rodent-to-human transmission.
7. Seventh, rodents are modelled without a latent stage because the extrinsic incubation period in the rodent host is short relative to the timescale of the model.
8. Finally, vertical transmission in mosquitoes is neglected because it is not a major driver of dengue transmission. These assumptions keep the model analytically tractable while retaining the essential transmission pathways.

3. Basic Properties of the Sub-Models

The dengue and Lassa fever sub-models are obtained from the full co-infection model by setting the compartments associated with the other disease to zero. Specifically, the dengue sub-model (7) is recovered from (4) by imposing $E_l = I_l = I_{dl} = T_{dl} = I_r = 0$, and the Lassa fever sub-model is recovered by imposing $E_d = I_d = I_{dl} = T_{dl} = I_v = 0$. This reduction preserves the structure of the full model in the following sense. The transmission terms for the retained disease are unchanged, because the forces of infection λ_d and λ_l depend only on the compartments of the corresponding disease. The progression, recovery and mortality terms are likewise unchanged, since no transition in (4) couples a dengue compartment to a Lassa fever compartment except through the co-infection variables, which are set to zero. Consequently, every solution of the sub-model is a solution of the full model restricted to the invariant subspace in which the compartments of the other disease vanish. This subspace is positively invariant because, when $E_l = I_l = I_{dl} = T_{dl} = I_r = 0$, the right-hand sides of the equations for these variables in (4) are zero or depend only on variables that are themselves zero. The reproduction numbers of the sub-models are therefore consistent with the full model in the limiting case where only one disease is present. In this section we examine each sub-model in turn.

3.1. Dengue Fever Sub-Model

The dengue sub-model is obtained from (4) by setting the Lassa fever compartments to zero. It consists of the following system of differential equations:

$$\begin{cases} \frac{dS_u}{dt} = \Lambda + \psi R - (\lambda_d + \epsilon + \mu_h)S_u, \\ \frac{dS_e}{dt} = \epsilon S_u - (\phi_1\lambda_d + \mu_h)S_e, \\ \frac{dE_d}{dt} = \lambda_d S_u + \phi_1\lambda_d S_e - (\sigma + \mu_h)E_d, \\ \frac{dI_d}{dt} = (1-\kappa)\sigma E_d - (\pi + \mu_h + d_d)I_d, \\ \frac{dR}{dt} = \sigma\kappa E_d + \pi I_d - (\psi + \mu_h)R, \\ \frac{dS_v}{dt} = \Omega_v - (\lambda_v + \mu_v)S_v, \\ \frac{dI_v}{dt} = \lambda_v S_v - \mu_v I_v, \end{cases} \tag{7}$$

the forces of infection are as in (5) and (6).

3.1.1. Disease-Free Equilibrium

The disease-free equilibrium of (7) is obtained by setting the right-hand sides of (7) to zero. This gives

$$\begin{aligned} \epsilon_d^0 &= \left(S_u^0, S_e^0, E_d^0, I_d^0, R^0, S_v^0, I_v^0\right) \\ &= \left(\frac{\Lambda}{\epsilon + \mu_h}, \frac{\Lambda\epsilon}{\mu_h(\epsilon + \mu_h)}, 0, 0, 0, \frac{\Omega_v}{\mu_v}, 0\right). \end{aligned} \tag{8}$$

3.1.2. Control Reproduction Number of the Dengue Sub-Model

The next-generation operator technique [33,34] is used to compute the control reproduction number, $\mathcal{R}_c^d = \rho(FV^{-1})$. The infected compartments are ordered as (E_d, I_d, I_v). The matrix F of new infection terms and the matrix V of remaining transition terms are constructed as follows:

$$F = \begin{bmatrix} 0 & 0 & \frac{\beta_{hd}(S_e\phi_1 + S_u)}{N_v} \\ 0 & 0 & 0 \\ 0 & \frac{\beta_v S_v}{N_h} & 0 \end{bmatrix}, \tag{9}$$

and

$$\begin{aligned} V &= \begin{bmatrix} k_1 & 0 & 0 \\ -(1-\kappa)\sigma & k_2 & 0 \\ 0 & 0 & \mu_v \end{bmatrix}, \\ \Rightarrow \quad V^{-1} &= \begin{bmatrix} {k_1}^{-1} & 0 & 0 \\ \frac{(1-\kappa)\sigma}{k_1 k_2} & {k_2}^{-1} & 0 \\ 0 & 0 & {\mu_v}^{-1} \end{bmatrix}. \end{aligned} \tag{10}$$

Since V is lower triangular with positive diagonal entries, it is invertible. Multiplying gives

$$FV^{-1} = \begin{bmatrix} 0 & 0 & \frac{\beta_{hd}(S_e\phi_1 + S_u)}{N_v\mu_v} \\ 0 & 0 & 0 \\ \frac{\beta_v S_v(1-\kappa)\sigma}{N_h k_1 k_2} & \frac{\beta_v S_v}{N_h k_2} & 0 \end{bmatrix}. \tag{11}$$

The only non-zero cycle in FV^{-1} runs from the exposed class to the vector class and back, so the spectral radius is the square root of the product of the two entries that close the cycle. Evaluating these entries at the disease-free equilibrium and simplifying gives

$$\mathcal{R}_c^d = \sqrt{\frac{\beta_{hd}\beta_v\sigma(1-\kappa)(\mu_h+\phi_1\epsilon)}{\mu_v k_1 k_2(\epsilon+\mu_h)}}. \tag{12}$$

Setting the control parameter to zero, $\phi_1 = 0$, yields the basic reproduction number

$$\mathcal{R}_0^d = \sqrt{\frac{\beta_{hd}\beta_v\sigma(1-\kappa)}{\mu_v k_1 k_2}}. \tag{13}$$

3.1.3. Endemic Equilibria of the Dengue Sub-Model

Let $(S_u^*, S_e^*, E_d^*, I_d^*, R^*, S_v^*, I_v^*)$ denote an equilibrium of (7). Setting the right-hand sides of (7) to zero and solving the resulting algebraic system gives

$$\begin{aligned}
S_u^* &= \frac{\Lambda((\phi_1\lambda_d+\mu_h)m_2m_3m_4)}{\lambda_d^2\eta_1+\lambda_d\eta_2+\eta_3}, S_e^* = \frac{\Lambda\epsilon m_2m_3m_4}{\lambda_d^2\eta_1+\lambda_d\eta_2+\eta_3},\\
E_d^* &= \frac{\Lambda\lambda_d((\phi_1\epsilon+\phi_1\lambda_d+\mu_h)m_3m_4)}{\lambda_d^2\eta_1+\lambda_d\eta_2+\eta_3},\\
I_d^* &= \frac{\Lambda\sigma\lambda_d(1-\kappa)((\phi_1\epsilon+\phi_1\lambda_d+\mu_h)m_4)}{\lambda_d^2\eta_1+\lambda_d\eta_2+\eta_3},\\
R^* &= \frac{\Lambda\lambda_d\sigma(\lambda_d\eta_4+\eta_5)}{\lambda_d^2\eta_1+\lambda_d\eta_2+\eta_3},\\
S_v^* &= \frac{\Omega_v}{\lambda_v+\mu_v}, \qquad I_v^* = \frac{\lambda_v\Omega_v}{\mu_v(\lambda_v+\mu_v)},
\end{aligned} \tag{14}$$

where

$$\begin{aligned}
m_1 &= \epsilon+\mu_h, \quad m_2 = \sigma+\mu_h, \quad m_3 = \pi+\mu_h+d_d, \quad m_4 = \psi+\mu_h,\\
\eta_1 &= \pi\psi\phi_1\sigma\kappa + \phi_1m_2m_3m_4 - \kappa\psi\phi_1\sigma m_3 - \pi\psi\phi_1,\\
\eta_2 &= \pi\epsilon\kappa\phi_1\psi\sigma - \epsilon\kappa m_3\phi_1\psi\sigma - \pi\epsilon\phi_1\psi\sigma + \pi\kappa\mu_h\psi\sigma - \kappa m_3\mu_h\psi\sigma\\
&\quad + m_1m_2m_3m_4\phi_1 - \pi\psi\sigma\mu_h - m_2m_3m_4\mu_h,\\
\eta_3 &= m_1m_2m_3m_4\mu_h,\\
\eta_4 &= \pi\kappa\phi_1 - \kappa m_3\phi_1 - \pi\phi_1,\\
\eta_5 &= \pi\epsilon\kappa\phi_1 - \epsilon\kappa m_3\phi_1 - \pi\epsilon\phi_1 + \pi\kappa\mu_h - \kappa m_3\mu_h - \pi\mu_h.
\end{aligned} \tag{15}$$

Since $m_i > 0$ for $i = 1,2,3,4$, the denominators are positive $\lambda_d^2\eta_1+\lambda_d\eta_2+\eta_3 > 0$ whenever $\eta_1, \eta_2, \eta_3 > 0$, and these inequalities are equivalent to

$$\begin{aligned}
\eta_1 > 0 &\iff \pi\psi\phi_1\sigma\kappa + \phi_1m_2m_3m_4 > \kappa\psi\phi_1\sigma m_3 + \pi\psi\phi_1,\\
\eta_2 > 0 &\iff \pi\epsilon\kappa\phi_1\psi\sigma + \pi\kappa\mu_h\psi\sigma + m_1m_2m_3m_4\phi_1\\
&\qquad > \epsilon\kappa m_3\phi_1\psi\sigma + \pi\epsilon\phi_1\psi\sigma + \kappa m_3\mu_h\psi\sigma + \pi\psi\sigma\mu_h + m_2m_3m_4\mu_h,\\
\eta_3 > 0 &\iff m_1m_2m_3m_4\mu_h > 0.
\end{aligned} \tag{16}$$

These conditions ensure that every equilibrium component is positive whenever the force of infection λ_d is positive.

Substituting I_d^* into λ_v^* gives the vector force of infection at equilibrium,

$$\lambda_v^* = \frac{\Gamma_4\lambda_d^{*2} + \Gamma_5\lambda_d^*}{\Gamma_1\lambda_d^{*2} + \Gamma_2\lambda_d^* + \Gamma_3}, \tag{17}$$

where

$$\begin{aligned}
\Gamma_1 &= \Lambda\phi_1 m_3 m_4 + \Lambda\sigma\phi_1(1-\kappa)m_4 + \Lambda\sigma\eta_1,\\
\Gamma_2 &= \Lambda\phi_1 m_2 m_3 m_4 + \Lambda\phi_1\epsilon m_3 m_4 + \Lambda\mu_h m_3 m_4\\
&\quad + \Lambda\sigma\phi_1(1-\kappa)\epsilon m_4 + \Lambda\sigma(1-\kappa)\mu_h m_4 + \Lambda\sigma\eta_5,\\
\Gamma_3 &= \Lambda\mu_h m_2 m_3 m_4 + \Lambda\epsilon m_2 m_3 m_4,\\
\Gamma_4 &= \beta_{hd}\Lambda\sigma\phi_1(1-\kappa)m_4,\\
\Gamma_5 &= \beta_{hd}\Lambda\sigma\phi_1(1-\kappa)\epsilon m_4 + \beta_{hd}\Lambda\sigma(1-\kappa)\mu_h m_4.
\end{aligned} \tag{18}$$

Substituting I_v^* gives

$$\begin{aligned}
&\mu_v\Gamma_1\lambda_v^*\lambda_d^{*3} + \mu_v\Gamma_2\lambda_v^*\lambda_d^{*2} + \mu_v\Gamma_3\lambda_v^*\lambda_d^* + \mu_v^2\Gamma_1\lambda_d^{*3}\\
&\quad + \mu_v^2\Gamma_2\lambda_d^{*2} + \mu_v^2\Gamma_3\lambda_d^* - \eta_1\beta_{hd}\Omega_v\lambda_v^*\lambda_d^{*2}\\
&\quad - \eta_2\beta_{hd}\Omega_v\lambda_v^*\lambda_d^* - \eta_3\beta_{hd}\Omega_v\lambda_v^* = 0.
\end{aligned} \tag{19}$$

Eliminating λ_v^* between (17) and (19) yields the quartic

$$B_1\lambda_d^{*4} + B_2\lambda_d^{*3} + B_3\lambda_d^{*2} + B_4\lambda_d^* + B_5 = 0, \tag{20}$$

where

$$\begin{aligned}
B_1 &= \mu_v\Gamma_1\Gamma_4 + \mu_v^2\Gamma_1^2,\\
B_2 &= \mu_v\Gamma_1\Gamma_4 + \mu_v\Gamma_2\Gamma_4 + 2\mu_v^2\Gamma_1\Gamma_3 - \eta_1\beta_{hd}\Omega_v\Gamma_4,\\
B_3 &= \mu_v\Gamma_2\Gamma_5 + \mu_v\Gamma_3\Gamma_4 + \mu_v^2\Gamma_1\Gamma_3 + \mu_v^2\Gamma_2\Gamma_2 + \mu_v^2\Gamma_1\Gamma_3\\
&\quad - \eta_1\Gamma_5\beta_{hd}\Omega_v - \eta_2\Gamma_4\beta_{hd}\Omega_v,\\
B_4 &= \mu_v\Gamma_3\Gamma_5 + 2\mu_v^2\Gamma_2\Gamma_3 - \eta_2\Gamma_5\beta_{hd}\Omega_v - \eta_3\Gamma_4\beta_{hd}\Omega_v,\\
B_5 &= (\mu_v\Lambda\mu_h m_2 m_3 m_4)^2(1+\epsilon)^2\Big(1 - \big(\mathcal{R}_c^d\big)^2\Big).
\end{aligned} \tag{21}$$

When $\mathcal{R}_c^d > 1$, the constant term satisfies $B_5 < 0$ while $B_1 > 0$. Since the polynomial in (20) is continuous and changes sign between $\lambda_d = 0$ and sufficiently large λ_d, it has at least one positive real root by the intermediate value theorem. Descartes' rule of signs then provides an upper bound on the number of such roots. This establishes the following result.

Theorem 1. *Whenever $\mathcal{R}_c^d > 1$, the dengue sub-model (7) has at least one endemic equilibrium.*

Proof. By the argument above, (20) has at least one positive real root when $\mathcal{R}_c^d > 1$. Each positive root λ_d^* determines a positive equilibrium through the expressions for $S_u^*, S_e^*, E_d^*, I_d^*, R^*, S_v^*, I_v^*$, so the sub-model admits at least one endemic equilibrium. □

For the stability analysis that follows, it is convenient to set $\psi = \kappa = 0$ in (7), which removes waning immunity and direct progression to the recovered class. The resulting system is

$$\begin{aligned}
\frac{dS_u}{dt} &= \Lambda - (\lambda_d + \epsilon + \mu_h)S_u,\\
\frac{dS_e}{dt} &= \epsilon S_u - (\phi_1\lambda_d + \mu_h)S_e,\\
\frac{dE_d}{dt} &= \lambda_d S_u + \phi_1\lambda_d S_e - (\sigma + \mu_h)E_d,\\
\frac{dI_d}{dt} &= \sigma E_d - (\pi + \mu_h + d_d)I_d,\\
\frac{dR}{dt} &= \pi I_d - \mu_h R,\\
\frac{dS_v}{dt} &= \Omega_v - (\lambda_v + \mu_v)S_v,\\
\frac{dI_v}{dt} &= \lambda_v S_v - \mu_v I_v.
\end{aligned} \tag{22}$$

The global stability result for (7) depends on (22) having a unique endemic equilibrium. If (22) admits a unique endemic equilibrium, the Lyapunov argument of the next section establishes global asymptotic stability; if it admits more than one, that argument does not apply.

Theorem 2. *The endemic equilibrium of the reduced dengue system (22) is globally asymptotically stable in the interior of the feasible region whenever $\mathcal{R}_c^d > 1$, provided that $\psi = \kappa = 0$.*

Proof. Consider the Goh–Volterra Lyapunov function

$$\begin{aligned}\mathcal{F} =& \left(S_u - S_u^{**} - S_u^{**}\ln\frac{S_u}{S_u^{**}}\right) + \left(S_e - S_e^{**} - S_e^{**}\ln\frac{S_e}{S_e^{**}}\right)\\ &+ \left(E_d - E_d^{**} - E_d^{**}\ln\frac{E_d}{E_d^{**}}\right)\\ &+ \frac{\sigma+\mu_h}{\sigma}\left(I_d - I_d^{**} - I_d^{**}\ln\frac{I_d}{I_d^{**}}\right)\\ &+ \frac{(\sigma+\mu_h)(\pi+\mu_h+d_d)}{\sigma\pi}\left(R - R^{**} - R^{**}\ln\frac{R}{R^{**}}\right)\\ &+ \left(S_v - S_v^{**} - S_v^{**}\ln\frac{S_v}{S_v^{**}}\right) + \left(I_v - I_v^{**} - I_v^{**}\ln\frac{I_v}{I_v^{**}}\right),\end{aligned} \tag{23}$$

which is positive definite in the neighbourhood of the endemic equilibrium $(S_u^{**}, S_e^{**}, E_d^{**}, I_d^{**}, R^{**}, S_v^{**}, I_v^{**})$. Differentiating (23) with respect to time gives

$$\begin{aligned}\dot{\mathcal{F}} =& \left(1 - \frac{S_u^{**}}{S_u}\right)\dot{S}_u + \left(1 - \frac{S_e^{**}}{S_e}\right)\dot{S}_e\\ &+ \left(1 - \frac{E_d^{**}}{E_d}\right)\dot{E}_d + \frac{\sigma+\mu_h}{\sigma}\left(1 - \frac{I_d^{**}}{I_d}\right)\dot{I}_d\\ &+ \frac{(\sigma+\mu_h)(\pi+\mu_h+d_d)}{\sigma\pi}\left(1 - \frac{R^{**}}{R}\right)\dot{R}\\ &+ \left(1 - \frac{S_v^{**}}{S_v}\right)\dot{S}_v + \left(1 - \frac{I_v^{**}}{I_v}\right)\dot{I}_v.\end{aligned} \tag{24}$$

Substituting the right-hand sides of (22) into (24) gives

$$\begin{aligned}\dot{\mathcal{F}} =& \left(1 - \frac{S_u^{**}}{S_u}\right)(\Lambda - \lambda_d S_u - (\epsilon+\mu_h)S_u)\\ &+ \left(1 - \frac{S_e^{**}}{S_e}\right)(\epsilon S_u - \phi_1\lambda_d S_e - \mu_h S_e)\\ &+ \left(1 - \frac{E_d^{**}}{E_d}\right)(\lambda_d S_u + \phi_1\lambda_d S_e - (\sigma+\mu_h)E_d)\\ &+ \frac{\sigma+\mu_h}{\sigma}\left(1 - \frac{I_d^{**}}{I_d}\right)(\sigma E_d - (\pi+\mu_h+d_d)I_d)\\ &+ \frac{(\sigma+\mu_h)(\pi+\mu_h+d_d)}{\sigma\pi}\left(1 - \frac{R^{**}}{R}\right)(\pi I_d - \mu_h R)\\ &+ \left(1 - \frac{S_v^{**}}{S_v}\right)(\Omega_v - \lambda_v S_v - \mu_v S_v)\\ &+ \left(1 - \frac{I_v^{**}}{I_v}\right)(\lambda_v S_v - \mu_v I_v).\end{aligned} \tag{25}$$

At the endemic equilibrium, the following relations hold:

$$\begin{aligned}
\Lambda &= \lambda_d^{**} S_u^{**} + (\epsilon + \mu_h) S_u^{**}, \\
\Omega_v &= \lambda_v^{**} S_v^{**} + \mu_v S_v^{**}, \\
\epsilon S_u^{**} &= \phi_1 \lambda_d^{**} S_e^{**} + \mu_h S_e^{**}, \\
(\sigma + \mu_h) E_d^{**} &= \lambda_d^{**} S_u^{**} + \phi_1 \lambda_d^{**} S_e^{**}, \\
\sigma E_d^{**} &= (\pi + \mu_h + d_d) I_d^{**}, \\
\mu_h R^{**} &= \pi I_d^{**}, \\
\mu_v I_v^{**} &= \lambda_v^{**} S_v^{**}.
\end{aligned} \tag{26}$$

Substituting (26) into (25) and grouping the resulting terms according to the equation of (22) from which they originate gives

$$\begin{aligned}
\dot{\mathcal{F}} \leq\ & (\epsilon + \mu_h) S_u^{**} \left(2 - \frac{S_u}{S_u^{**}} - \frac{S_u^{**}}{S_u} \right) + \mu_h S_e^{**} \left(2 - \frac{S_e}{S_e^{**}} - \frac{S_e^{**}}{S_e} \right) \\
& + \lambda_d^{**} S_u^{**} \left(3 - \frac{S_u^{**}}{S_u} - \frac{S_u E_d^{**}}{S_u^{**} E_d} - \frac{E_d I_d^{**}}{E_d^{**} I_d} \right) \\
& + \phi_1 \lambda_d^{**} S_e^{**} \left(3 - \frac{S_e^{**}}{S_e} - \frac{S_e E_d^{**}}{S_e^{**} E_d} - \frac{E_d I_d^{**}}{E_d^{**} I_d} \right) \\
& + \mu_h R^{**} \left(2 - \frac{R}{R^{**}} - \frac{R^{**}}{R} \right) \\
& + \mu_v S_v^{**} \left(2 - \frac{S_v}{S_v^{**}} - \frac{S_v^{**}}{S_v} \right) + \lambda_v^{**} S_v^{**} \left(3 - \frac{S_v^{**}}{S_v} - \frac{I_v}{I_v^{**}} - \frac{S_v I_v^{**}}{S_v^{**} I_v} \right).
\end{aligned} \tag{27}$$

Each bracket in (27) has product one, and is therefore non-positive by the arithmetic–geometric mean inequality, with equality if and only if all the ratios in that bracket equal one. Explicitly,

$$\begin{aligned}
& \frac{S_u}{S_u^{**}} \cdot \frac{S_u^{**}}{S_u} = 1, \qquad \frac{S_e}{S_e^{**}} \cdot \frac{S_e^{**}}{S_e} = 1, \\
& \frac{S_u^{**}}{S_u} \cdot \frac{S_u E_d^{**}}{S_u^{**} E_d} \cdot \frac{E_d I_d^{**}}{E_d^{**} I_d} = 1, \\
& \frac{S_e^{**}}{S_e} \cdot \frac{S_e E_d^{**}}{S_e^{**} E_d} \cdot \frac{E_d I_d^{**}}{E_d^{**} I_d} = 1, \\
& \frac{R}{R^{**}} \cdot \frac{R^{**}}{R} = 1, \qquad \frac{S_v}{S_v^{**}} \cdot \frac{S_v^{**}}{S_v} = 1, \\
& \frac{S_v^{**}}{S_v} \cdot \frac{I_v}{I_v^{**}} \cdot \frac{S_v I_v^{**}}{S_v^{**} I_v} = 1.
\end{aligned} \tag{28}$$

Hence, each bracket is non-positive, and $\dot{\mathcal{F}} \leq 0$, with equality only when $S_u = S_u^{**}$, $S_e = S_e^{**}$, $E_d = E_d^{**}$, $I_d = I_d^{**}$, $R = R^{**}$, $S_v = S_v^{**}$ and $I_v = I_v^{**}$, that is, only at the endemic equilibrium.

By LaSalle's invariance principle [35], every solution of (22) that remains in the feasible region converges to the largest invariant subset of $\{\dot{\mathcal{F}} = 0\}$. By the equality condition above, this subset is the endemic equilibrium itself. Therefore,

$$\lim_{t \to \infty} (S_u(t), S_e(t), E_d(t), I_d(t), R(t), S_v(t), I_v(t)) = \left(S_u^{**}, S_e^{**}, E_d^{**}, I_d^{**}, R^{**}, S_v^{**}, I_v^{**} \right), \tag{29}$$

so the dengue endemic equilibrium is globally asymptotically stable whenever it exists and $\psi = \kappa = 0$. □

The condition $\psi = \kappa = 0$ in Theorem 2 requires comment. It is imposed for analytical convenience rather than from biological necessity. Setting $\psi = 0$ removes the feedback from

the recovered class to the uneducated susceptible class, which would otherwise introduce terms into the Lyapunov derivative that cannot be signed without further assumptions on the relative magnitudes of the parameters. Setting $\kappa = 0$ removes the direct progression from the exposed class to the recovered class, which would add a further positive term to the derivative of the Lyapunov function for the same reason. With both conditions imposed, the Goh–Volterra function (23) is well defined and its derivative is non-positive by the arithmetic–geometric mean inequality, as the proof shows.

The restriction means that Theorem 2 establishes global asymptotic stability of the endemic equilibrium of the reduced system (22), not of every parameter regime of the full dengue sub-model. This is a genuine limitation, and we do not claim otherwise. Removing the restriction would require a different method of proof, which we leave for future work. The global result under $\psi = \kappa = 0$ should therefore be read as establishing stability of the endemic equilibrium for a restricted but biologically meaningful parameter set, rather than as a general statement about the full sub-model.

3.2. Lassa Fever Sub-Model

The Lassa fever sub-model is obtained from (4) by setting the dengue compartments to zero. It consists of the following system of differential equations:

$$\begin{cases} \frac{dS_u}{dt} = \Lambda + \psi R - (\lambda_l + \epsilon + \mu_h)S_u, \\ \frac{dS_e}{dt} = \epsilon S_u - (\phi_2\lambda_l + \mu_h)S_e, \\ \frac{dE_l}{dt} = \lambda_l S_u + \phi_2\lambda_l S_e - (\alpha + \mu_h)E_l, \\ \frac{dI_l}{dt} = (1-\kappa)\alpha E_l - (\eta + \mu_h + d_l)I_l, \\ \frac{dR}{dt} = \alpha\kappa E_l + \eta I_l - (\psi + \mu_h)R, \\ \frac{dS_r}{dt} = \Omega_r - (\lambda_r + \mu_r)S_r, \\ \frac{dI_r}{dt} = \lambda_r S_r - \mu_r I_r, \end{cases} \tag{30}$$

where the forces of infection for humans and rodents are

$$\lambda_l = \frac{\beta_{hl} I_r}{N_r} \tag{31}$$

and

$$\lambda_r = \frac{\beta_r I_l}{N_h}, \tag{32}$$

respectively.

3.2.1. Disease-Free Equilibrium of the Lassa Fever Sub-Model

The disease-free equilibrium of (30) is obtained by setting the right-hand sides of (30) to zero. This gives

$$\begin{aligned} \epsilon_l^0 &= (S_u^0, S_e^0, E_l^0, I_l^0, R^0, S_r^0, I_r^0) \\ &= \left(\frac{\Lambda}{\epsilon + \mu_h}, \frac{\Lambda\epsilon}{\mu_h(\epsilon + \mu_h)}, 0, 0, 0, \frac{\Omega_r}{\mu_r}, 0\right). \end{aligned} \tag{33}$$

3.2.2. Control Reproduction Number of the Lassa Fever Sub-Model

The next-generation operator technique [33,34] is used to compute the control reproduction number, $\mathcal{R}_c^l = \rho(FV^{-1})$. The infected compartments are ordered as (E_l, I_l, I_r).

The matrix F of new infection terms and the matrix V of remaining transition terms are constructed as follows:

$$F = \begin{bmatrix} 0 & 0 & \frac{\beta_{hl}(S_e\phi_2+S_u)}{N_r} \\ 0 & 0 & 0 \\ 0 & \frac{\beta_r S_r}{N_h} & 0 \end{bmatrix}, \tag{34}$$

and

$$V = \begin{bmatrix} k_3 & 0 & 0 \\ -(1-\kappa)\alpha & k_4 & 0 \\ 0 & 0 & \mu_r \end{bmatrix}. \tag{35}$$

Since V is lower triangular with positive diagonal entries, it is invertible, and

$$V^{-1} = \begin{bmatrix} {k_3}^{-1} & 0 & 0 \\ \frac{(1-\kappa)\alpha}{k_3 k_4} & {k_4}^{-1} & 0 \\ 0 & 0 & {\mu_r}^{-1} \end{bmatrix}. \tag{36}$$

Multiplying gives

$$FV^{-1} = \begin{bmatrix} 0 & 0 & \frac{\beta_{hl}(S_e\phi_2+S_u)}{N_r\mu_r} \\ \frac{\beta_r S_r(1-\kappa)\alpha}{N_h k_3 k_4} & 0 & 0 \\ 0 & 0 & 0 \end{bmatrix}. \tag{37}$$

The only non-zero cycle in FV^{-1} runs from the exposed class to the rodent class and back, so the spectral radius is the square root of the product of the two entries that close the cycle. Evaluating these entries at the disease-free equilibrium and simplifying gives

$$\mathcal{R}_c^l = \sqrt{\frac{\beta_{hl}\beta_r\alpha(1-\kappa)(\mu_h+\phi_2\epsilon)}{\mu_r k_3 k_4(\epsilon+\mu_h)}}.$$

Setting the control parameter to zero, $\phi_2 = 0$, yields the basic reproduction number

$$\mathcal{R}_0^l = \sqrt{\frac{\beta_{hl}\beta_r\alpha(1-\kappa)}{\mu_r k_3 k_4}}.$$

3.2.3. Endemic Equilibria of the Lassa Fever Sub-Model

Let $(S_u^*, S_e^*, E_l^*, I_l^*, R^*, S_r^*, I_r^*)$ denote an equilibrium of (30). Setting the right-hand sides of (30) to zero and solving the resulting algebraic system gives

$$\begin{aligned} S_u^* &= \frac{\Lambda((\phi_2\lambda_l+\mu_h)n_2n_3n_4)}{\lambda_l^2\chi_1+\lambda_l\chi_2+\chi_3}, S_e^* = \frac{\Lambda\epsilon n_2n_3n_4}{\lambda_l^2\chi_1+\lambda_l\chi_2+\chi_3}, \\ E_l^* &= \frac{\Lambda\lambda_l((\phi_2\epsilon+\phi_2\lambda_l+\mu_h)n_3n_4)}{\lambda_l^2\chi_1+\lambda_l\chi_2+\chi_3}, \\ I_l^* &= \frac{\Lambda\alpha\lambda_l(1-\kappa)((\phi_2\epsilon+\phi_2\lambda_l+\mu_h)n_4)}{\lambda_l^2\chi_1+\lambda_l\chi_2+\chi_3}, \\ R^* &= \frac{\Lambda\lambda_l\alpha(\lambda_l\chi_4+\chi_5)}{\lambda_l^2\chi_1+\lambda_l\chi_2+\chi_3}, \\ S_r^* &= \frac{\Omega_r}{\lambda_r+\mu_r}, \qquad I_r^* = \frac{\lambda_r\Omega_r}{\mu_r(\lambda_r+\mu_r)}, \end{aligned} \tag{38}$$

where

$$\begin{aligned}
n_1 &= \epsilon + \mu_h, \quad n_2 = \alpha + \mu_h, \quad n_3 = \eta + \mu_h + d_l, \quad n_4 = \psi + \mu_h,\\
\chi_1 &= \eta\psi\phi_2\alpha\kappa + \phi_2 n_2 n_3 n_4 - \kappa\psi\phi_2\alpha n_3 - \eta\psi\phi_2,\\
\chi_2 &= \eta\epsilon\kappa\phi_2\psi\alpha - \epsilon\kappa n_3\phi_2\psi\alpha - \eta\epsilon\phi_2\psi\alpha + \eta\kappa\mu_h\psi\alpha - \kappa n_3\mu_h\psi\alpha\\
&\quad + n_1 n_2 n_3 n_4\phi_2 - \eta\psi\alpha\mu_h - n_2 n_3 n_4\mu_h,\\
\chi_3 &= n_1 n_2 n_3 n_4\mu_h,\\
\chi_4 &= \eta\kappa\phi_2 - \kappa n_3\phi_2 - \eta\phi_2,\\
\chi_5 &= \eta\epsilon\kappa\phi_2 - \epsilon\kappa n_3\phi_2 - \eta\epsilon\phi_2 + \eta\kappa\mu_h - \kappa n_3\mu_h - \eta\mu_h.
\end{aligned} \tag{39}$$

Since $n_i > 0$ for $i = 1,2,3,4$, the denominators satisfy $\lambda_l^2\chi_1 + \lambda_l\chi_2 + \chi_3 > 0$ whenever $\chi_1, \chi_2, \chi_3 > 0$, which holds under the conditions

$$\begin{aligned}
\chi_1 > 0 &\iff \eta\psi\phi_2\alpha\kappa + \phi_2 n_2 n_3 n_4 > \kappa\psi\phi_2\alpha n_3 + \eta\psi\phi_2,\\
\chi_2 > 0 &\iff \eta\epsilon\kappa\phi_2\psi\alpha + n_1 n_2 n_3 n_4\phi_2\\
&\qquad > \epsilon\kappa n_3\phi_2\psi\alpha + \eta\epsilon\phi_2\psi\alpha + \eta\kappa\mu_h\psi\alpha + \kappa n_3\mu_h\psi\alpha + \eta\psi\alpha\mu_h + n_2 n_3 n_4\mu_h,\\
\chi_3 > 0 &\iff n_1 n_2 n_3 n_4\mu_h > 0.
\end{aligned} \tag{40}$$

These conditions ensure that every equilibrium component is positive whenever the force of infection λ_l is positive.

Substituting I_l^* into (32) gives the rodent force of infection at equilibrium,

$$\lambda_r^* = \frac{\Phi_4\lambda_l^{*2} + \Phi_5\lambda_l^*}{\Phi_1\lambda_l^{*2} + \Phi_2\lambda_l^* + \Phi_3}, \tag{41}$$

where

$$\begin{aligned}
\Phi_1 &= \Lambda\phi_2 n_3 n_4 + \Lambda\alpha\phi_2(1-\kappa)n_4 + \Lambda\alpha\chi_1,\\
\Phi_2 &= \Lambda\phi_2 n_2 n_3 n_4 + \Lambda\phi_2\epsilon n_3 n_4 + \Lambda\mu_h n_3 n_4\\
&\quad + \Lambda\alpha\phi_2(1-\kappa)\epsilon n_4 + \Lambda\alpha(1-\kappa)\mu_h n_4 + \Lambda\alpha\chi_5,\\
\Phi_3 &= \Lambda\mu_h n_2 n_3 n_4 + \Lambda\epsilon n_2 n_3 n_4,\\
\Phi_4 &= \beta_{hl}\Lambda\alpha\phi_2(1-\kappa)n_4,\\
\Phi_5 &= \beta_{hl}\Lambda\alpha\phi_2(1-\kappa)\epsilon n_4 + \beta_{hl}\Lambda\alpha(1-\kappa)\mu_h n_4.
\end{aligned} \tag{42}$$

Substituting I_r^* into (31) gives

$$\begin{aligned}
&\mu_r\Phi_1\lambda_r^*\lambda_l^{*3} + \mu_r\Phi_2\lambda_r^*\lambda_l^{*2} + \mu_r\Phi_3\lambda_r^*\lambda_l^* + \mu_r^2\Phi_1\lambda_l^{*3}\\
&\quad + \mu_r^2\Phi_2\lambda_l^{*2} + \mu_r^2\Phi_3\lambda_l^* - \chi_1\beta_{hl}\Omega_r\lambda_r^*\lambda_l^{*2}\\
&\quad - \chi_2\beta_{hl}\Omega_r\lambda_r^*\lambda_l^* - \chi_3\beta_{hl}\Omega_r\lambda_r^* = 0.
\end{aligned} \tag{43}$$

Eliminating λ_r^* between (41) and (43) yields the quartic

$$A_1\lambda_l^{*4} + A_2\lambda_l^{*3} + A_3\lambda_l^{*2} + A_4\lambda_l^* + A_5 = 0, \tag{44}$$

where

$$\begin{aligned}
A_1 &= \mu_r\Phi_1\Phi_4 + \mu_r^2\Phi_1^2,\\
A_2 &= \mu_r\Phi_1\Phi_4 + \mu_r\Phi_2\Phi_4 + 2\mu_r^2\Phi_1\Phi_3 - \chi_1\beta_{hl}\Omega_r\Phi_4,\\
A_3 &= \mu_r\Phi_2\Phi_5 + \mu_r\Phi_3\Phi_4 + \mu_r^2\Phi_1\Phi_3 + \mu_r^2\Phi_2\Phi_2\\
&\quad + \mu_r^2\Phi_1\Phi_3 - \chi_1\Phi_5\beta_{hl}\Omega_r - \chi_2\Phi_4\beta_{hl}\Omega_r,\\
A_4 &= \mu_r\Phi_3\Phi_5 + 2\mu_r^2\Phi_2\Phi_3 - \chi_2\Phi_5\beta_{hl}\Omega_r - \chi_3\Phi_4\beta_{hl}\Omega_r,\\
A_5 &= (\mu_r\Lambda\mu_h n_2 n_3 n_4)^2(1+\epsilon)^2\Big(1 - \big(\mathcal{R}_c^l\big)^2\Big).
\end{aligned} \tag{45}$$

When $\mathcal{R}_c^l > 1$, the constant term satisfies $A_5 < 0$ while $A_1 > 0$. Since the polynomial in (44) is continuous and changes sign between $\lambda_l = 0$ and sufficiently large λ_l, it has at least one positive real root by the intermediate value theorem. Descartes' rule of signs then provides an upper bound on the number of such roots. This establishes the following result.

Theorem 3. *Whenever $\mathcal{R}_c^l > 1$, the Lassa fever sub-model (30) has at least one endemic equilibrium.*

Proof. By the argument above, (44) has at least one positive real root when $\mathcal{R}_c^l > 1$. Each positive root λ_l^* determines a positive equilibrium through the expressions for $S_u^*, S_e^*, E_l^*, I_l^*, R^*, S_r^*, I_r^*$, so the sub-model admits at least one endemic equilibrium. □

For the stability analysis that follows, it is convenient to set $\psi = \kappa = 0$ in (30), which removes waning immunity and direct progression to the recovered class. The resulting system is

$$\begin{aligned}
\frac{dS_u}{dt} &= \Lambda - (\lambda_l + \epsilon + \mu_h)S_u, \\
\frac{dS_e}{dt} &= \epsilon S_u - (\phi_2\lambda_l + \mu_h)S_e, \\
\frac{dE_l}{dt} &= \lambda_l S_u + \phi_2\lambda_l S_e - (\alpha + \mu_h)E_l, \\
\frac{dI_l}{dt} &= \alpha E_l - (\eta + \mu_h + d_l)I_l, \\
\frac{dR}{dt} &= \eta I_l - \mu_h R, \\
\frac{dS_r}{dt} &= \Omega_r - (\lambda_r + \mu_r)S_r, \\
\frac{dI_r}{dt} &= \lambda_r S_r - \mu_r I_r.
\end{aligned} \tag{46}$$

The global stability result for (30) depends on (46) having a unique endemic equilibrium. If (46) admits a unique endemic equilibrium, the Lyapunov argument of the next section establishes global asymptotic stability; if it admits more than one, that argument does not apply.

Theorem 4. *The endemic equilibrium of the reduced Lassa fever system (46) is globally asymptotically stable in the interior of the feasible region whenever $\mathcal{R}_c^l > 1$, provided that $\psi = \kappa = 0$.*

Proof. Consider the Goh–Volterra Lyapunov function

$$\begin{aligned}
\mho_l = &\left(S_u - S_u^{**} - S_u^{**}\ln\frac{S_u}{S_u^{**}}\right) + \left(S_e - S_e^{**} - S_e^{**}\ln\frac{S_e}{S_e^{**}}\right) \\
&+ \left(E_l - E_l^{**} - E_l^{**}\ln\frac{E_l}{E_l^{**}}\right) + \frac{\alpha+\mu_h}{\alpha}\left(I_l - I_l^{**} - I_l^{**}\ln\frac{I_l}{I_l^{**}}\right) \\
&+ \frac{(\alpha+\mu_h)(\eta+\mu_h+d_l)}{\alpha\eta}\left(R - R^{**} - R^{**}\ln\frac{R}{R^{**}}\right) \\
&+ \left(S_r - S_r^{**} - S_r^{**}\ln\frac{S_r}{S_r^{**}}\right) + \left(I_r - I_r^{**} - I_r^{**}\ln\frac{I_r}{I_r^{**}}\right),
\end{aligned} \tag{47}$$

which is positive definite in the neighbourhood of the endemic equilibrium $(S_u^{**}, S_e^{**}, E_l^{**}, I_l^{**}, R^{**}, S_r^{**}, I_r^{**})$. Differentiating (47) with respect to time gives

$$\begin{aligned}
\dot{\mho}_l = &\left(1 - \frac{S_u^{**}}{S_u}\right)\dot{S}_u + \left(1 - \frac{S_e^{**}}{S_e}\right)\dot{S}_e + \left(1 - \frac{E_l^{**}}{E_l}\right)\dot{E}_l \\
&+ \frac{\alpha+\mu_h}{\alpha}\left(1 - \frac{I_l^{**}}{I_l}\right)\dot{I}_l \\
&+ \frac{(\alpha+\mu_h)(\eta+\mu_h+d_l)}{\alpha\eta}\left(1 - \frac{R^{**}}{R}\right)\dot{R} \\
&+ \left(1 - \frac{S_r^{**}}{S_r}\right)\dot{S}_r + \left(1 - \frac{I_r^{**}}{I_r}\right)\dot{I}_r.
\end{aligned} \tag{48}$$

Substituting the right-hand sides of (46) into (48) gives

$$\begin{aligned}
\dot{\mho}_l = &\left(1-\frac{S_u^{**}}{S_u}\right)(\Lambda-\lambda_l S_u-(\epsilon+\mu_h)S_u)\\
&+\left(1-\frac{S_e^{**}}{S_e}\right)(\epsilon S_u-\phi_2\lambda_l S_e-\mu_h S_e)\\
&+\left(1-\frac{E_l^{**}}{E_l}\right)(\lambda_l S_u+\phi_2\lambda_l S_e-(\alpha+\mu_h)E_l)\\
&+\frac{\alpha+\mu_h}{\alpha}\left(1-\frac{I_l^{**}}{I_l}\right)(\alpha E_l-(\eta+\mu_h+d_l)I_l)\\
&+\frac{(\alpha+\mu_h)(\eta+\mu_h+d_l)}{\alpha\eta}\left(1-\frac{R^{**}}{R}\right)(\eta I_l-\mu_h R)\\
&+\left(1-\frac{S_r^{**}}{S_r}\right)(\Omega_r-\lambda_r S_r-\mu_r S_r)\\
&+\left(1-\frac{I_r^{**}}{I_r}\right)(\lambda_r S_r-\mu_r I_r).
\end{aligned} \tag{49}$$

At the endemic equilibrium, the following relations hold:

$$\begin{aligned}
\Lambda &= \lambda_l^{**}S_u^{**}+(\epsilon+\mu_h)S_u^{**},\\
\Omega_r &= \lambda_r^{**}S_r^{**}+\mu_r S_r^{**},\\
\epsilon S_u^{**} &= \phi_2\lambda_l^{**}S_e^{**}+\mu_h S_e^{**},\\
(\alpha+\mu_h)E_l^{**} &= \lambda_l^{**}S_u^{**}+\phi_2\lambda_l^{**}S_e^{**},\\
\alpha E_l^{**} &= (\eta+\mu_h+d_l)I_l^{**},\\
\mu_h R^{**} &= \eta I_l^{**},\\
\mu_r I_r^{**} &= \lambda_r^{**}S_r^{**}.
\end{aligned} \tag{50}$$

Substituting (50) into (49) and grouping the resulting terms according to the equation of (46) from which they originate gives

$$\begin{aligned}
\dot{\mho}_l \le\ &(\epsilon+\mu_h)S_u^{**}\left(2-\frac{S_u}{S_u^{**}}-\frac{S_u^{**}}{S_u}\right)+\mu_h S_e^{**}\left(2-\frac{S_e}{S_e^{**}}-\frac{S_e^{**}}{S_e}\right)\\
&+\lambda_l^{**}S_u^{**}\left(4-\frac{S_u^{**}}{S_u}-\frac{S_u E_l^{**}}{S_u^{**}E_l}-\frac{E_l I_l^{**}}{E_l^{**}I_l}-\frac{I_l}{I_l^{**}}\right)\\
&+\phi_2\lambda_l^{**}S_e^{**}\left(4-\frac{S_e^{**}}{S_e}-\frac{S_e E_l^{**}}{S_e^{**}E_l}-\frac{E_l I_l^{**}}{E_l^{**}I_l}-\frac{I_l}{I_l^{**}}\right)\\
&+\mu_h R^{**}\left(2-\frac{R}{R^{**}}-\frac{R^{**}}{R}\right)\\
&+\mu_r S_r^{**}\left(2-\frac{S_r}{S_r^{**}}-\frac{S_r^{**}}{S_r}\right)+\lambda_r^{**}S_r^{**}\left(3-\frac{S_r^{**}}{S_r}-\frac{I_r}{I_r^{**}}-\frac{S_r I_r^{**}}{S_r^{**}I_r}\right).
\end{aligned} \tag{51}$$

Each bracket in (51) has product one, and is therefore non-positive by the arithmetic–geometric mean inequality, with equality if and only if all the ratios in that bracket equal one. Explicitly,

$$\begin{aligned}
&\frac{S_u}{S_u^{**}} \cdot \frac{S_u^{**}}{S_u} = 1, \qquad \frac{S_e}{S_e^{**}} \cdot \frac{S_e^{**}}{S_e} = 1,\\
&\frac{S_u^{**}}{S_u} \cdot \frac{S_u E_l^{**}}{S_u^{**} E_l} \cdot \frac{E_l I_l^{**}}{E_l^{**} I_l} \cdot \frac{I_l}{I_l^{**}} = 1,\\
&\frac{S_e^{**}}{S_e} \cdot \frac{S_e E_l^{**}}{S_e^{**} E_l} \cdot \frac{E_l I_l^{**}}{E_l^{**} I_l} \cdot \frac{I_l}{I_l^{**}} = 1,\\
&\frac{R}{R^{**}} \cdot \frac{R^{**}}{R} = 1, \qquad \frac{S_r}{S_r^{**}} \cdot \frac{S_r^{**}}{S_r} = 1,\\
&\frac{S_r^{**}}{S_r} \cdot \frac{I_r}{I_r^{**}} \cdot \frac{S_r I_r^{**}}{S_r^{**} I_r} = 1.
\end{aligned} \tag{52}$$

Hence, each bracket is non-positive, and $\dot{\mho}_l \leq 0$, with equality only when $S_u = S_u^{**}$, $S_e = S_e^{**}$, $E_l = E_l^{**}$, $I_l = I_l^{**}$, $R = R^{**}$, $S_r = S_r^{**}$ and $I_r = I_r^{**}$, that is, only at the endemic equilibrium.

By LaSalle's invariance principle [35], every solution of (46) that remains in the feasible region converges to the largest invariant subset of $\{\dot{\mho}_l = 0\}$. By the equality condition above, this subset is the endemic equilibrium itself. Therefore,

$$\lim_{t\to\infty}(S_u(t), S_e(t), E_l(t), I_l(t), R(t), S_r(t), I_r(t)) = \left(S_u^{**}, S_e^{**}, E_l^{**}, I_l^{**}, R^{**}, S_r^{**}, I_r^{**}\right), \tag{53}$$

so the Lassa fever endemic equilibrium is globally asymptotically stable whenever it exists and $\psi = \kappa = 0$. □

As with Theorem 2, the condition $\psi = \kappa = 0$ in Theorem 4 is imposed for analytical convenience rather than from biological necessity. Setting $\psi = 0$ decouples the recovered class from the uneducated susceptible class, and setting $\kappa = 0$ removes the direct progression from the exposed class to the recovered class; without these restrictions the derivative of the Goh–Volterra function contains terms that cannot be signed. The theorem therefore establishes global asymptotic stability of the endemic equilibrium of the reduced system (46), not of every parameter regime of the full Lassa fever sub-model. This is a genuine limitation, and removing it would require a different method of proof, which we leave for future work.

4. Basic Properties of the Co-Infection Model

4.1. Boundedness and Positivity

Theorem 5. *The closed set,*

$$D = \left\{S_u, S_e, E_d, E_l, I_d, I_l, I_{dl}, T_{dl}, R \in R_+^9 : N_h \leq \frac{\Lambda}{\mu_h}\right\}, \tag{54}$$

is positively invariant and attracts all positive solutions of the model.

Proof. The total human population of the model (4) is

$$\begin{aligned}
N_h(t) =& S_u(t) + S_e(t) + E_d(t) + E_l(t) + I_d(t) + I_l(t)\\
&+ I_{dl}(t) + T_{dl}(t) + R(t)
\end{aligned} \tag{55}$$

Differentiating N_h both sides of (55) and substitute in (4), we get

$$\frac{dN_h}{dt} = \Lambda - \mu_h N_h - d_d I_d - d_l I_l - d_{dl}(I_{dl} + T_{dl}), \tag{56}$$

using the comparison theorem, we have

$$\frac{dN_h}{dt} = \Lambda - \mu_h N_h, \tag{57}$$

solving (57) gives

$$N_h(t) \leq \frac{\Lambda}{\mu_h} + \left[N_h(0) - \frac{\Lambda}{\mu_h}\right]e^{-\mu_h t}. \tag{58}$$

Similarly, recall that from (2)

$$\frac{N_v}{dt} = \frac{S_v}{dt} + \frac{I_v}{dt}. \tag{59}$$

Differentiating both sides of (59) we have

$$N_v(t) \leq \frac{\Omega_v}{\mu_v} + \left[N_v(0) - \frac{\Omega_v}{\mu_v}\right]e^{-\mu_v t}, \tag{60}$$

and similarly,

$$N_r(t) \leq \frac{\Omega_r}{\mu_r} + \left[N_r(0) - \frac{\Omega_r}{\mu_r}\right]e^{-\mu_r t}. \tag{61}$$

Now, from (58),$N_h(t) \to N_h(0)$ as $t \to 0 \Rightarrow N_h(t) \leq \frac{\Lambda}{\mu_h}$ and as $t \to \infty, N_h(t) \to \frac{\Lambda}{\mu_h}$ Similarly, (60),$N_v(t) \to N_v(0)$ as $t \to 0 \Rightarrow N_v(t) \leq \frac{\Omega_v}{\mu_v}$ and as $t \to \infty, N_v(t) \to \frac{\Omega}{\mu_v}$ and (61),$N_r(t) \to N_r(0)$ as $t \to 0 \Rightarrow N_r(t) \leq \frac{\Omega_r}{\mu_r}$ and as $t \to \infty, N_r(t) \to \frac{\Omega_r}{\mu_r}$. □

4.2. Disease Free Equilibrium Point

The model (4) has a disease-free equilibrium point by setting the right-hand side of (4) to zero.

$$\epsilon^0 = \left(\frac{\Lambda}{\epsilon + \mu_h}, \frac{\Lambda\epsilon}{\mu_h(\epsilon + \mu_h)}, 0, 0, \frac{\Omega_v}{\mu_v}, 0, 0, 0, \frac{\Omega_r}{\mu_r}, 0, 0, 0, 0\right). \tag{62}$$

4.3. Basic Reproduction Number

The next-generation operator technique [34] is used to compute the control reproduction number, $\mathcal{R}_c = \rho(FV^{-1})$. The infected compartments are ordered as

$$(E_d,\ I_d,\ E_l,\ I_l,\ I_{dl},\ T_{dl},\ I_v,\ I_r),$$

so that rows and columns 1 to 8 correspond to these compartments in this order. The matrix F of new infection terms and the matrix V of remaining transition terms are constructed as follows.

Four types of new infection appear in the model: dengue infection of humans, at rate $\lambda_d = \beta_{hd} I_v / N_v$, which enters the equation for E_d; Lassa fever infection of humans, at rate $\lambda_l = \beta_{hl} I_r / N_r$, which enters the equation for E_l; dengue infection of mosquitoes, at rate $\lambda_v = \beta_v I_d / N_h$, which enters the equation for I_v; and Lassa fever infection of rodents, at rate $\lambda_r = \beta_r I_l / N_h$, which enters the equation for I_r. In the ordering above, these correspond to the entries $(1,7)$, $(3,8)$, $(7,2)$ and $(8,4)$ of F, respectively. No other compartment receives new infections. The co-infection terms $\lambda_l I_d$ and $\lambda_d I_l$ are nonlinear in the infected variables and do not appear in F; they are retained in the nonlinear part of the vector field.

$$F = \begin{bmatrix} 0 & 0 & 0 & 0 & 0 & 0 & \psi_1 & 0 \\ 0 & 0 & 0 & 0 & 0 & 0 & 0 & 0 \\ 0 & 0 & 0 & 0 & 0 & 0 & 0 & \psi_2 \\ 0 & 0 & 0 & 0 & 0 & 0 & 0 & 0 \\ 0 & 0 & 0 & 0 & 0 & 0 & 0 & 0 \\ 0 & 0 & 0 & 0 & 0 & 0 & 0 & 0 \\ 0 & \frac{\beta_v S_v}{N_h} & 0 & 0 & 0 & 0 & 0 & 0 \\ 0 & 0 & 0 & \frac{\beta_r S_r}{N_h} & 0 & 0 & 0 & 0 \end{bmatrix}, \tag{63}$$

where

$$\psi_1 = \frac{\beta_{hd}(S_u + \phi_1 S_e)}{N_v}, \qquad \psi_2 = \frac{\beta_{hl}(S_u + \phi_2 S_e)}{N_r}. \tag{64}$$

The matrix V contains the linear transition terms: progression from exposed to infectious for each disease, treatment, recovery and mortality. Its diagonal entries are k_1 to k_6 for the six human infected compartments and μ_v, μ_r for the vector and rodent compartments. The off-diagonal entries are the negative of the inflow terms from other infected compartments: $-(1-\kappa)\sigma$ from E_d to I_d, $-(1-\kappa)\alpha$ from E_l to I_l, and $-\xi$ from I_{dl} to T_{dl}.

$$V = \begin{bmatrix} k_1 & 0 & 0 & 0 & 0 & 0 & 0 & 0 \\ -(1-\kappa)\sigma & k_2 & 0 & 0 & 0 & 0 & 0 & 0 \\ 0 & 0 & k_3 & 0 & 0 & 0 & 0 & 0 \\ 0 & 0 & -(1-\kappa)\alpha & k_4 & 0 & 0 & 0 & 0 \\ 0 & 0 & 0 & 0 & k_5 & 0 & 0 & 0 \\ 0 & 0 & 0 & 0 & -\xi & k_6 & 0 & 0 \\ 0 & 0 & 0 & 0 & 0 & 0 & \mu_v & 0 \\ 0 & 0 & 0 & 0 & 0 & 0 & 0 & \mu_r \end{bmatrix}, \tag{65}$$

where

$$k_1 = \sigma + \mu_h, \quad k_2 = \pi + \mu_h + d_d, \quad k_3 = \alpha + \mu_h, \quad k_4 = \eta + \mu_h + d_l, \quad k_5 = \xi + \mu_h + d_{dl}, \quad k_6 = \tau + \mu_h + d_{dl}. \tag{66}$$

Since V is lower triangular with positive diagonal entries, it is invertible. Its inverse is

$$V^{-1} = \begin{bmatrix} \frac{1}{k_1} & 0 & 0 & 0 & 0 & 0 & 0 & 0 \\ \frac{(1-\kappa)\sigma}{k_1 k_2} & \frac{1}{k_2} & 0 & 0 & 0 & 0 & 0 & 0 \\ 0 & 0 & \frac{1}{k_3} & 0 & 0 & 0 & 0 & 0 \\ 0 & 0 & \frac{(1-\kappa)\alpha}{k_3 k_4} & \frac{1}{k_4} & 0 & 0 & 0 & 0 \\ 0 & 0 & 0 & 0 & \frac{1}{k_5} & 0 & 0 & 0 \\ 0 & 0 & 0 & 0 & \frac{\xi}{k_5 k_6} & \frac{1}{k_6} & 0 & 0 \\ 0 & 0 & 0 & 0 & 0 & 0 & \frac{1}{\mu_v} & 0 \\ 0 & 0 & 0 & 0 & 0 & 0 & 0 & \frac{1}{\mu_r} \end{bmatrix}. \tag{67}$$

Each off-diagonal entry is the product of the corresponding transition rate and the reciprocals of the two diagonal entries it connects, which follows from the lower-triangular structure of V. All off-diagonal entries are positive because $1-\kappa > 0$, $\alpha > 0$, $\sigma > 0$ and $\xi > 0$.

Multiplying F by V^{-1} gives

$$FV^{-1} = \begin{bmatrix} 0 & 0 & 0 & 0 & 0 & 0 & \frac{\psi_1}{\mu_v} & 0 \\ 0 & 0 & 0 & 0 & 0 & 0 & 0 & 0 \\ 0 & 0 & 0 & 0 & 0 & 0 & 0 & \frac{\psi_2}{\mu_r} \\ 0 & 0 & 0 & 0 & 0 & 0 & 0 & 0 \\ 0 & 0 & 0 & 0 & 0 & 0 & 0 & 0 \\ 0 & 0 & 0 & 0 & 0 & 0 & 0 & 0 \\ \frac{\beta_v S_v(1-\kappa)\sigma}{N_h k_1 k_2} & \frac{\beta_v S_v}{N_h k_2} & 0 & 0 & 0 & 0 & 0 & 0 \\ 0 & 0 & \frac{\beta_r S_r(1-\kappa)\alpha}{N_h k_3 k_4} & \frac{\beta_r S_r}{N_h k_4} & 0 & 0 & 0 & 0 \end{bmatrix}. \tag{68}$$

The only non-zero cycles in FV^{-1} are $1 \to 7 \to 1$ and $3 \to 8 \to 3$, corresponding to the dengue and Lassa fever transmission cycles respectively. The spectral radius is therefore the maximum of the square roots of the two cycle products,

$$\mathcal{R}_c = \rho(FV^{-1}) = \max\{\mathcal{R}_c^d,\ \mathcal{R}_c^l\}, \tag{69}$$

where

$$\mathcal{R}_c^d = \sqrt{\frac{\beta_{hd}\beta_v\sigma(1-\kappa)(S_u+\phi_1 S_e)S_v}{N_v N_h k_1 k_2 \mu_v}}, \qquad \mathcal{R}_c^l = \sqrt{\frac{\beta_{hl}\beta_r\alpha(1-\kappa)(S_u+\phi_2 S_e)S_r}{N_r N_h k_3 k_4 \mu_r}}. \tag{70}$$

Evaluating at the disease-free equilibrium, where $S_u^0 = \Lambda/(\epsilon+\mu_h)$, $S_e^0 = \Lambda\epsilon/[\mu_h(\epsilon+\mu_h)]$, $S_v^0 = \Omega_v/\mu_v$, $S_r^0 = \Omega_r/\mu_r$, $N_v^0 = \Omega_v/\mu_v$, $N_r^0 = \Omega_r/\mu_r$ and $N_h^0 = S_u^0 + S_e^0$, gives

$$\mathcal{R}_c^d = \sqrt{\frac{\beta_{hd}\beta_v\sigma(1-\kappa)(\mu_h+\epsilon\phi_1)}{\mu_v k_1 k_2(\epsilon+\mu_h)}}, \qquad \mathcal{R}_c^l = \sqrt{\frac{\beta_{hl}\beta_r\alpha(1-\kappa)(\mu_h+\epsilon\phi_2)}{\mu_r k_3 k_4(\epsilon+\mu_h)}}. \tag{71}$$

The basic reproduction numbers of the two sub-models are obtained by setting the control parameters $\phi_1 = \phi_2 = 0$, which gives

$$\mathcal{R}_0^d = \sqrt{\frac{\beta_{hd}\beta_v\sigma(1-\kappa)}{\mu_v k_1 k_2}}, \qquad \mathcal{R}_0^l = \sqrt{\frac{\beta_{hl}\beta_r\alpha(1-\kappa)}{\mu_r k_3 k_4}}. \tag{72}$$

4.4. Global Stability of Disease-Free Equilibrium

Theorem 6. *The disease-free equilibrium ϵ^* of model (4) is globally asymptotically stable in the feasible region whenever $\mathcal{R}_c^d \le 1$, $\mathcal{R}_c^l \le 1$, and the two inequalities (89) and (90) hold.*

Proof. Consider the linear Lyapunov function

$$L = P_1E_d + P_2I_d + P_3I_v + P_4E_l + P_5I_l + P_6I_r + P_7I_{dl} + P_8T_{dl}. \tag{73}$$

Differentiating (73) along solutions of (4) gives

$$\begin{aligned} \frac{dL}{dt} &= P_1\dot{E}_d + P_2\dot{I}_d + P_3\dot{I}_v + P_4\dot{E}_l + P_5\dot{I}_l + P_6\dot{I}_r + P_7\dot{I}_{dl} + P_8\dot{T}_{dl} \\ &= P_1(\lambda_d S_u + \phi_1\lambda_d S_e - k_1E_d) + P_2((1-\kappa)\sigma E_d - (\pi+\lambda_l+\mu_h+d_d)I_d) \\ &\quad + P_3(\lambda_v S_v - \mu_v I_v) + P_4(\lambda_l S_u + \phi_2\lambda_l S_e - k_3E_l) \\ &\quad + P_5((1-\kappa)\alpha E_l - (\eta+\lambda_d+\mu_h+d_l)I_l) + P_6(\lambda_r S_r - \mu_r I_r) \\ &\quad + P_7(\lambda_l I_d + \lambda_d I_l - k_5 I_{dl}) + P_8(\xi I_{dl} - k_6 T_{dl}). \end{aligned} \tag{74}$$

Substituting the forces of infection $\lambda_d = \beta_{hd} I_v / N_v$, $\lambda_l = \beta_{hl} I_r / N_r$, $\lambda_v = \beta_v I_d / N_h$ and $\lambda_r = \beta_r I_l / N_h$, and grouping the terms by compartment, gives

$$\begin{aligned}\frac{dL}{dt} &= (P_2(1-\kappa)\sigma - P_1 k_1)E_d + (P_5(1-\kappa)\alpha - P_4 k_3)E_l \\ &+ \left(P_3 \frac{\beta_v S_v}{N_h} - P_2 k_2\right) I_d + \left(P_6 \frac{\beta_r S_r}{N_h} - P_5 k_4\right) I_l \\ &+ \left(P_1 \frac{\beta_{hd}(S_u + \phi_1 S_e)}{N_v} - P_3 \mu_v\right) I_v + \left(P_4 \frac{\beta_{hl}(S_u + \phi_2 S_e)}{N_r} - P_6 \mu_r\right) I_r \\ &+ (-P_7 k_5 + P_8 \xi) I_{dl} - P_8 k_6 T_{dl} + P_7 \frac{\beta_{hl} I_r}{N_r} I_d + P_7 \frac{\beta_{hd} I_v}{N_v} I_l.\end{aligned} \tag{75}$$

At the disease-free equilibrium, $S_u^0 = \Lambda/(\epsilon + \mu_h)$, $S_e^0 = \Lambda\epsilon/[\mu_h(\epsilon + \mu_h)]$, $S_v^0 = \Omega_v/\mu_v$, $S_r^0 = \Omega_r/\mu_r$ and $N_h^0 = S_u^0 + S_e^0$, so that

$$\frac{\beta_v S_v^0}{N_h^0} = \frac{\beta_v \Omega_v \mu_h}{\Lambda \mu_v}, \qquad \frac{\beta_r S_r^0}{N_h^0} = \frac{\beta_r \Omega_r \mu_h}{\Lambda \mu_r}, \tag{76}$$

and

$$\frac{\beta_{hd}(S_u^0 + \phi_1 S_e^0)}{N_v^0} = \frac{\beta_{hd}\Lambda(\mu_h + \epsilon\phi_1)}{\mu_h(\epsilon + \mu_h)} \cdot \frac{\mu_v}{\Omega_v}, \qquad \frac{\beta_{hl}(S_u^0 + \phi_2 S_e^0)}{N_r^0} = \frac{\beta_{hl}\Lambda(\mu_h + \epsilon\phi_2)}{\mu_h(\epsilon + \mu_h)} \cdot \frac{\mu_r}{\Omega_r}. \tag{77}$$

Following the original proof, we choose

$$P_1 = \mu_v k_2, \tag{78}$$

$$P_2 = \left(\frac{\beta_{hd}\Lambda(\mu_h + \epsilon\phi_1)}{\mu_h(\epsilon + \mu_h)} \cdot \frac{\mu_v}{\Omega_v}\right) \frac{\beta_v \Omega_v \mu_h}{\Lambda \mu_v}, \tag{79}$$

$$P_3 = \left(\frac{\beta_{hd}\Lambda(\mu_h + \epsilon\phi_1)}{\mu_h(\epsilon + \mu_h)} \cdot \frac{\mu_v}{\Omega_v}\right) k_2, \tag{80}$$

$$P_4 = \mu_r k_4, \tag{81}$$

$$P_5 = \left(\frac{\beta_{hl}\Lambda(\mu_h + \epsilon\phi_2)}{\mu_h(\epsilon + \mu_h)} \cdot \frac{\mu_r}{\Omega_r}\right) \frac{\beta_r \Omega_r \mu_h}{\Lambda \mu_r}, \tag{82}$$

$$P_6 = \left(\frac{\beta_{hl}\Lambda(\mu_h + \epsilon\phi_2)}{\mu_h(\epsilon + \mu_h)} \cdot \frac{\mu_r}{\Omega_r}\right) k_4, \tag{83}$$

$$P_7 = k_5, \qquad P_8 = \frac{\xi k_5}{k_6}, \tag{84}$$

with $k_1 = \sigma + \mu_h$, $k_2 = \pi + \mu_h + d_d$, $k_3 = \alpha + \mu_h$, $k_4 = \eta + \mu_h + d_l$, $k_5 = \xi + \mu_h + d_{dl}$ and $k_6 = \tau + \mu_h + d_{dl}$. Note that P_5 and P_6 are expressed in terms of the Lassa fever parameters, correcting the earlier version in which the dengue parameters appeared.

With these choices, the coefficients of E_d, E_l, I_v and I_r in (75) vanish by construction: each is the difference between an inflow term and the corresponding removal term, and the weights are chosen so that the two are equal. What remains is

$$\frac{dL}{dt} = \left(P_3 \frac{\beta_v S_v^0}{N_h^0} - P_2 k_2\right) I_d + \left(P_6 \frac{\beta_r S_r^0}{N_h^0} - P_5 k_4\right) I_l + \left(-k_5^2 + \frac{\xi^2 k_5}{k_6}\right) I_{dl} - \frac{\xi^2 k_5}{k_6} T_{dl} + k_5 \frac{\beta_{hl} I_r}{N_r} I_d + k_5 \frac{\beta_{hd} I_v}{N_v} I_l. \tag{85}$$

Substituting (76) into the coefficients of I_d and I_l, and factoring $k_2 P_2$ from the first and $k_4 P_5$ from the second, gives

$$\begin{aligned}\frac{dL}{dt} &= P_2k_2\left(\frac{\beta_{hd}\beta_v(1-\kappa)\sigma(\mu_h+\epsilon\phi_1)}{\mu_v k_1 k_2(\epsilon+\mu_h)}-1\right)I_d + P_5k_4\left(\frac{\beta_{hl}\beta_r(1-\kappa)\alpha(\mu_h+\epsilon\phi_2)}{\mu_r k_3 k_4(\epsilon+\mu_h)}-1\right)I_l \\ &\quad + \left(-k_5^2+\frac{\xi^2k_5}{k_6}\right)I_{dl} - \frac{\xi^2k_5}{k_6}T_{dl} + k_5\frac{\beta_{hl}I_r}{N_r}I_d + k_5\frac{\beta_{hd}I_v}{N_v}I_l \\ &= P_2k_2\big((\mathcal{R}_c^d)^2-1\big)I_d + P_5k_4\big((\mathcal{R}_c^l)^2-1\big)I_l - k_5^2\left(1-\frac{\xi^2}{k_5k_6}\right)I_{dl} - \frac{\xi^2k_5}{k_6}T_{dl} \\ &\quad + k_5\frac{\beta_{hl}I_r}{N_r}I_d + k_5\frac{\beta_{hd}I_v}{N_v}I_l.\end{aligned} \tag{86}$$

Since $I_r \le N_r$ and $I_v \le N_v$, the last two terms satisfy

$$k_5\frac{\beta_{hl}I_r}{N_r}I_d + k_5\frac{\beta_{hd}I_v}{N_v}I_l \le k_5\beta_{hl}I_d + k_5\beta_{hd}I_l. \tag{87}$$

Combining (86) and (87),

$$\begin{aligned}\frac{dL}{dt} &\le \big[P_2k_2\big((\mathcal{R}_c^d)^2-1\big)+k_5\beta_{hl}\big]I_d + \big[P_5k_4\big((\mathcal{R}_c^l)^2-1\big)+k_5\beta_{hd}\big]I_l \\ &\quad - k_5^2\left(1-\frac{\xi^2}{k_5k_6}\right)I_{dl} - \frac{\xi^2k_5}{k_6}T_{dl}.\end{aligned} \tag{88}$$

Every coefficient in (88) is non-positive provided $\mathcal{R}_c^d \le 1$, $\mathcal{R}_c^l \le 1$, and

$$k_5\beta_{hl} \le P_2k_2\big(1-(\mathcal{R}_c^d)^2\big), \tag{89}$$

$$k_5\beta_{hd} \le P_5k_4\big(1-(\mathcal{R}_c^l)^2\big). \tag{90}$$

The third coefficient is negative for all positive parameters, because $k_5k_6 > \xi^2$ follows from $k_5 = \xi + \mu_h + d_{dl}$ and $k_6 = \tau + \mu_h + d_{dl}$, and the fourth is negative. Hence, $\frac{dL}{dt} \le 0$, with equality only when $E_d = E_l = I_d = I_l = I_{dl} = T_{dl} = I_v = I_r = 0$. Inserting these values into (4) gives $\dot{S}_u = \Lambda - (\epsilon+\mu_h)S_u$, $\dot{S}_e = \epsilon S_u - \mu_h S_e$, $\dot{S}_v = \Omega_v - \mu_v S_v$ and $\dot{S}_r = \Omega_r - \mu_r S_r$, whose only invariant set is the disease-free equilibrium ϵ^0. By LaSalle's invariance principle [35], every solution of (4) converges to ϵ^0. □

5. Estimation of Biological Parameters: Least-Squares Technique

To ensure that the proposed model reflects the observed epidemiology, the parameters of the Lassa fever sub-model (30) that cannot be taken reliably from the literature were estimated from Nigerian surveillance data by bounded nonlinear least squares, while the remaining parameters were fixed. Below we describe the data, the objective function, the estimated and fixed parameters, the bounds and initial guesses, the optimisation algorithm and its convergence criteria, the goodness of fit, the uncertainty of the estimates and their practical identifiability, in sufficient detail for the procedure to be reproduced. The dengue sub-model (7) can be fitted to the NCDC dengue data and analysed in exactly the same way (Section 5.8).

5.1. Data

Weekly numbers of confirmed Lassa fever cases in Nigeria were taken from the Lassa fever situation reports of the Nigeria Centre for Disease Control and Prevention (NCDC) [36] for the 16 consecutive epidemiological weeks from week 52 of 2023 to week 15 of 2024 (Table 3). The quantity fitted was the cumulative number of confirmed cases counted from week 52 of 2023, which rises from 43 to 767. No report was available for week 9 of 2024 (shown as "–" in the NCDC series). The cumulative count for that week is therefore not an observation, and week 9 was excluded from the objective function, leaving $N = 15$ data points.

Table 3. Weekly NCDC Lassa fever data used for parameter estimation (Nigeria, epidemiological week 52 of 2023 to week 15 of 2024). The cumulative values $\tilde{y}_j$ were fitted; $t_j = j$ weeks.

j	Epi-Week	New Confirmed Cases	Cumulative Confirmed Cases, $\tilde{y}_j$
0	52/2023	43	43
1	01/2024	53	96
2	02/2024	81	177
3	03/2024	77	254
4	04/2024	47	301
5	05/2024	70	371
6	06/2024	83	454
7	07/2024	66	520
8	08/2024	96	616
9	09/2024	–	616 *
10	10/2024	50	666
11	11/2024	35	701
12	12/2024	25	726
13	13/2024	15	741
14	14/2024	11	752
15	15/2024	15	767

* No report for week 9 of 2024; excluded from the fit.

5.2. Model Output and Objective Function

Let $\mathbf{x}(t;\boldsymbol{\theta}) = (S_u, S_e, E_l, I_l, R, S_r, I_r)$ denote the solution of the Lassa fever sub-model (31)–(33) for the parameter vector $\boldsymbol{\theta}$. All rates are expressed per week and time is measured in weeks, $t_j = j$ being the end of epidemiological week j, $j = 0, 1, \ldots, 15$. Only individuals who develop symptoms enter the class I_l and can be confirmed and reported, whereas the fraction κ of exposed individuals recovers without symptoms. To compare the model with the reported counts, the sub-model was therefore augmented with the cumulative number of symptomatic cases $C(t)$,

$$\frac{dC}{dt} = (1-\kappa)\,\alpha\,E_l(t), \qquad C(t_0) = \tilde{y}_0 = 43, \tag{91}$$

whose right-hand side is the rate at which new cases enter I_l in (31). The model prediction for week j is $y_j(\boldsymbol{\theta}) = C(t_j;\boldsymbol{\theta})$.

The parameters were estimated by minimising the sum of squared errors (SSE) between observed and predicted cumulative cases,

$$\begin{aligned} \hat{\boldsymbol{\theta}} &= \arg\min_{\boldsymbol{\ell}\le\boldsymbol{\theta}\le\boldsymbol{u}} \mathrm{SSE}(\boldsymbol{\theta}), \\ \mathrm{SSE}(\boldsymbol{\theta}) &= \sum_{j\in\mathcal{J}} \Big(\tilde{y}_j - y_j(\boldsymbol{\theta})\Big)^2, \qquad \mathcal{J} = \{0,1,\ldots,15\} \setminus \{9\}, \end{aligned} \tag{92}$$

where $\tilde{y}_j$ is the observed cumulative count in week j (Table 3), $N = |\mathcal{J}| = 15$, and $\boldsymbol{\ell}$ and $\boldsymbol{u}$ are the lower and upper bounds in Table 4. The residuals were unweighted. Since the mean squared error MSE = SSE/N differs from the SSE only by a constant factor, both have the same minimiser.

Table 4. Estimated parameters: admissible bounds and initial guesses (rates per week).

Parameter	Lower	Upper	Initial Guess	Description
β_{hl}	0	10	0.5	human infection rate
β_r	0	50	1	human-to-rodent transmission rate
κ	0	1	0.8	proportion of asymptomatic recoveries

5.3. Estimated and Fixed Parameters

Three parameters were estimated simultaneously: the human infection rate β_{hl}, the human-to-rodent transmission rate β_r and the proportion κ of exposed individuals who recover without developing symptoms, $\boldsymbol{\theta} = (\beta_{hl}, \beta_r, \kappa)$. These parameters determine the size and timing of the reported epidemic and are poorly known for the Nigerian setting. Their bounds and initial guesses are given in Table 4: the transmission rates were constrained to be non-negative, with upper bounds of 10 and 50 per week (the wider bound for β_r reflects the small rodent population in the initial conditions), and κ to lie in $[0, 1]$.

All other parameters were fixed at the values in Table 5. They describe demography, the natural history of infection and the awareness compartment, and were assumed as follows: a human life expectancy of 55 years, loss of immunity after one year on average, an incubation period of 10 days ($\alpha = 0.7$ per week), an infectious period of two weeks ($\eta = 0.5$ per week), a disease-induced death rate $d_l = 0.1$ per week, corresponding to a case-fatality ratio $d_l/(\eta+\mu_h+d_l) \approx 17\%$ among symptomatic cases, and a rodent lifespan of one year. The recruitment rates were set to $\Lambda = \mu_h N_h(0)$ and $\Omega_r = \mu_r N_r(0)$, so that the human and rodent populations are at demographic equilibrium at $t = 0$. A preliminary analysis showed that a fourth estimated parameter cannot be determined from 15 cumulative counts. Estimating ϕ_2 in addition drove it to its lower bound without a meaningful change in the SSE. Estimating α or η gave pairwise correlations of 0.999 and 0.986, respectively, with the transmission rates. Estimating μ_r lowered the SSE but left all four parameters poorly determined, with pairwise correlations up to 0.99 and relative standard errors of 21–259%. These parameters were therefore fixed. The initial conditions were

$$\begin{aligned} &S_u(0) = 11978, \quad S_e(0) = 102, \quad E_l(0) = 230, \quad I_l(0) = 200, \\ &R(0) = 22, \quad S_r(0) = 50, \quad I_r(0) = 31, \end{aligned} \tag{93}$$

so that $N_h(0) = 12532$ and $N_r(0) = 81$.

Table 5. Fixed parameter values used in the Lassa fever sub-model and in the full model (rates per week). The upper block lists the parameters of the Lassa fever sub-model; the lower block lists the parameters of the full co-infection model that do not enter the Lassa fever sub-model but are needed for the sensitivity analysis and the simulations.

Parameter	Value	Description	Source
Lassa fever sub-model			
μ_h	3.485×10^{-4}	natural death rate of humans, $1/(55 \times 52.18)$	[3]
Λ	4.367	recruitment rate of humans, $\mu_h N_h(0)$	computed
ψ	0.01916	rate of loss of immunity, $1/52.18$	assumed
ϵ	0.01	rate of transfer from S_u to S_e	[37]
ϕ_2	0.5	relative susceptibility of S_e	assumed
Lassa fever sub-model			
α	0.7	progression rate from E_l (incubation period 10 days)	[38]
η	0.5	recovery rate of I_l (infectious period 2 weeks)	[37]
d_l	0.1	Lassa fever-induced death rate	assumed
μ_r	0.01916	natural death rate of rodents, $1/52.18$	[38]
Ω_r	1.552	recruitment rate of rodents, $\mu_r N_r(0)$	computed
Parameters of the full model not used in the Lassa fever sub-model			
μ_v	0.5	natural death rate of mosquitoes	[38]
Ω_v	5.0×10^4	recruitment rate of mosquitoes	[39]
σ	0.667	progression rate from E_d to I_d	[37]

Table 5. *Cont.*

Parameter	Value	Description	Source
ϕ_1	0.134381	relative susceptibility of S_e to dengue (dimensionless)	[38]
π	0.205996	treatment rate of I_d	[38]
d_d	0.203716	dengue-induced death rate	[38]
ξ	0.5	rate of transfer from I_{dl} to T_{dl}	assumed
d_{dl}	0.0032	co-infection-induced death rate	assumed
τ	0.09	recovery rate of T_{dl}	assumed
β_{hd}	0.000041	dengue infection rate of humans	[38]
β_v	0.018093	dengue infection rate of mosquitoes	[38]

5.4. Numerical Procedure

All computations were carried out in MATLAB R2024b with the Optimization Toolbox. The augmented system (30), (91) was integrated with `ode45` (relative tolerance 10^{-8}, absolute tolerance 10^{-10}, non-negativity of all state variables enforced). Problem (92) was solved with `lsqnonlin` using the trust-region-reflective algorithm [40,41], which handles the box constraints directly; the Jacobian of the residuals was approximated by forward finite differences with relative step 10^{-5}. The optimisation was terminated as soon as one of the following held: change in the SSE below `FunctionTolerance` $= 10^{-8}$, step size below `StepTolerance` $= 10^{-8}$, first-order optimality measure below `OptimalityTolerance` $= 10^{-8}$, 5000 function evaluations, or 1000 iterations.

To reduce the risk of convergence to a local minimum, the optimisation was started from the initial guess in Table 4 and from four additional starting points drawn by Latin hypercube sampling within the bounds (random seed 2024). All five runs converged and reached the same minimum (relative difference in SSE below 10^{-6}). The best run stopped because the change in the SSE fell below the function tolerance, after 20 iterations and 84 function evaluations.

5.5. Goodness of Fit

The quality of the fit was quantified by the SSE in (92) and by

$$\mathrm{RMSE} = \sqrt{\frac{\mathrm{SSE}}{N}}, \qquad \mathrm{MAE} = \frac{1}{N}\sum_{j\in\mathcal{J}} |\tilde{y}_j - y_j|, \qquad R^2 = 1 - \frac{\mathrm{SSE}}{\sum_{j\in\mathcal{J}}(\tilde{y}_j - \bar{\tilde{y}})^2}, \tag{94}$$

together with the small-sample Akaike information criterion $\mathrm{AIC}_c = N\ln(\mathrm{SSE}/N) + 2p + 2p(p+1)/(N-p-1)$, where $p = 3$ is the number of estimated parameters [42]. The values are given in Table 6. The fitted curve follows the data closely over the whole period (Figure 2); the RMSE of 17.0 cases is about 2% of the final cumulative count of 767. The residuals (Figure 3) lie between -27.1 and 35.9 cases and change sign several times. The largest residual occurs in week 8, immediately before the missing week-9 report, which suggests that some week-9 cases may have been reported in week 8. The summary statistics of the observed and fitted series are almost identical (Table 7).

Table 6. Goodness-of-fit measures of the least-squares fit of the Lassa fever sub-model ($N = 15$, $p = 3$).

Measure	Value
SSE	4334.27
MSE	288.95
RMSE	17.00
MAE	14.01
R^2	0.9953
AIC_c	93.18

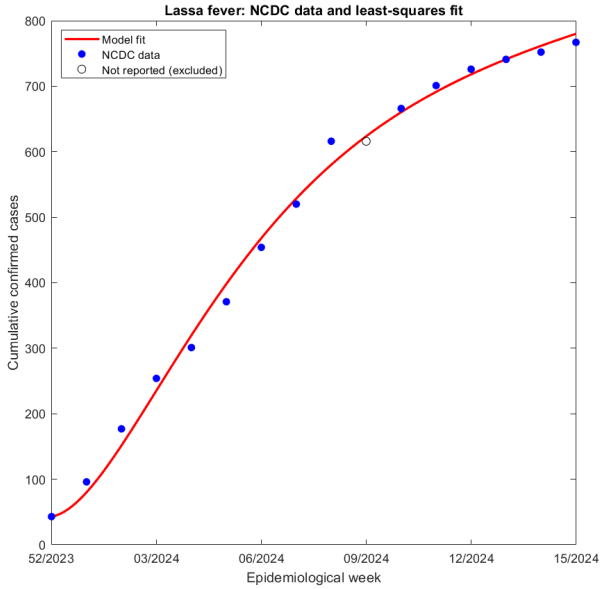


Figure 2. Cumulative confirmed Lassa fever cases reported by NCDC (blue circles) and the best-fitting solution of the Lassa fever sub-model (red line). The open circle marks week 9 of 2024, for which no report was available and which was excluded from the fit.

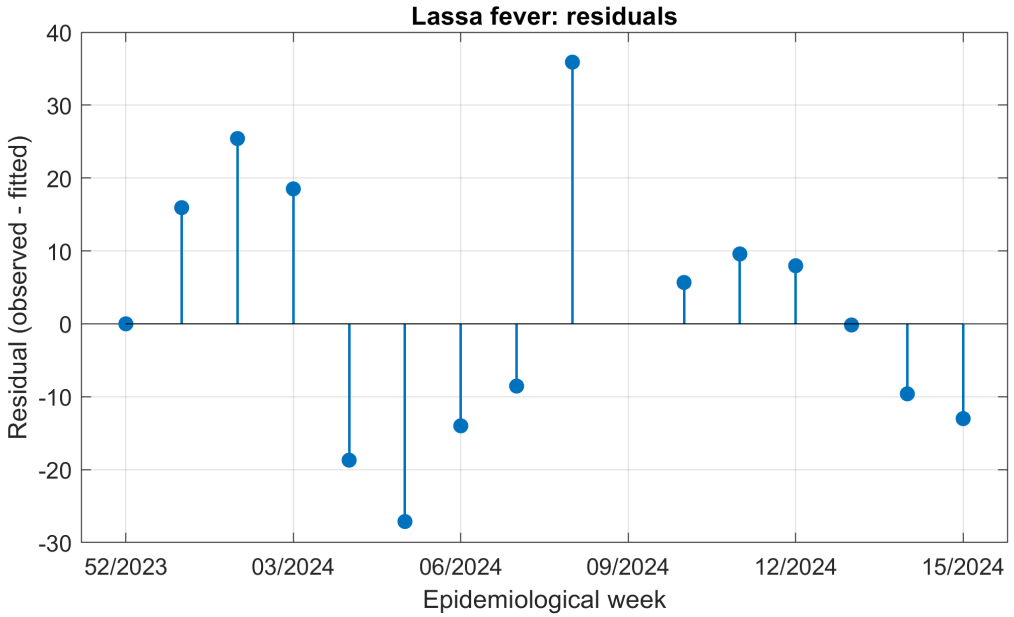


Figure 3. Residuals $\tilde{y}_j - y_j(\hat{\boldsymbol{\theta}})$ of the least-squares fit of the Lassa fever sub-model.

Table 7. Summary statistics of the observed and fitted cumulative Lassa fever cases (15 reported weeks).

Statistic	Observed Data	Predicted Data
Minimum	43.0	43.0
Q1	277.5	277.6
Q2 (Median)	520.0	528.5
Q3	713.5	704.7
Mean	479.0	477.1
Maximum	767.0	780.0
Standard deviation	255.6	258.4

5.6. Uncertainty of the Estimated Parameters

Uncertainty in $\hat{\boldsymbol{\theta}}$ was quantified by a parametric bootstrap [43]. From the best-fitting curve, the expected number of new cases in each week, $\Delta y_j = y_j(\hat{\boldsymbol{\theta}}) - y_{j-1}(\hat{\boldsymbol{\theta}})$, was computed. $B = 100$ synthetic data sets were generated by drawing each weekly count from a Poisson distribution with mean Δy_j and accumulating the draws, and the model was refitted to every synthetic data set with the same bounds and settings as above, starting from $\hat{\boldsymbol{\theta}}$. The 2.5th and 97.5th percentiles of the refitted values give the 95% confidence interval of each parameter, and the coefficient of variation $\mathrm{CV} = \mathrm{sd}/\hat{\theta} \times 100\%$ of the bootstrap distribution measures its relative precision. As a check, asymptotic 95% intervals $\hat{\theta}_i \pm t_{0.975,\,N-p}\,\mathrm{se}_i$ were computed from the covariance matrix $\widehat{\sigma}^2(\mathbf{J}^\top\mathbf{J})^{-1}$, where $\mathbf{J}$ is the Jacobian of the residuals at $\hat{\boldsymbol{\theta}}$ and $\widehat{\sigma}^2 = \mathrm{SSE}/(N-p)$.

The estimates and their confidence intervals are listed in Table 8, and the bootstrap distributions are shown in Figure 4. The human infection rate is $\hat{\beta}_{hl} = 0.409$ per week (95% bootstrap CI $[0.295, 0.517]$, CV 15.7%). The proportion of asymptomatic recoveries is $\hat{\kappa} = 0.943$ ($[0.935, 0.947]$, CV 0.3%), i.e., only about 6% of exposed individuals develop symptoms and are reported, consistent with the large share of mild or undetected Lassa fever infections. Both parameters are well determined. In contrast, the human-to-rodent transmission rate $\hat{\beta}_r = 10.4$ per week has a bootstrap interval of $[0.05, 37.0]$ that spans almost the whole admissible range (CV 102.8%), and its asymptotic interval includes negative values; β_r is therefore not determined by the data (Section 5.7).

Table 8. Estimated parameters of the Lassa fever sub-model (rates per week) with 95% asymptotic, bootstrap ($B = 100$) and profile-likelihood confidence intervals, bootstrap coefficient of variation and practical identifiability.

Parameter	Estimate	95% Asymptotic CI	95% Bootstrap CI [b]	CV (%)	95% Profile CI [a]	Identifiable
β_{hl}	0.4094	[0.2215, 0.5973]	[0.2948, 0.5170]	15.7	[0.2495, 0.4990]	Yes
β_r	10.40	[−16.09, 36.90]	[0.0516, 37.01]	102.8	[0, 50]	No
κ	0.9430	[0.9378, 0.9483]	[0.9350, 0.9469]	0.3	[0.9383, 0.9430]	Yes

[a] Outermost grid points below the threshold; the limits are accurate to the grid spacing. [b] The profile stays below the threshold over the whole admissible interval.

5.7. Practical Identifiability

Because only 15 observations of a single output are available, the practical identifiability of the estimated parameters was assessed in three complementary ways.

1. *Local sensitivity analysis.* The rank and condition number of the normalised sensitivity matrix $\mathbf{S} = \mathbf{J}\,\mathrm{diag}(\hat{\boldsymbol{\theta}})$ were computed; a rank smaller than p, or a very large condition number, indicates that some combinations of parameters cannot be determined from the data.
2. *Parameter correlations.* The correlation matrix derived from $(\mathbf{J}^\top\mathbf{J})^{-1}$ was inspected; pairs with $|\rho_{ij}| > 0.95$ were regarded as practically non-identifiable individually.
3. *Profile likelihood* [44]. For each parameter θ_i, the profile

$$\mathrm{PL}(\theta_i) = \min_{\boldsymbol{\theta}_{-i}} N \ln\big(\mathrm{SSE}(\boldsymbol{\theta})/N\big),$$

was computed on a grid of 35–45 points spanning its admissible interval and refined near $\hat{\theta}_i$, re-optimising the other two parameters at each grid point from three starting points. A parameter was declared practically identifiable if its profile exceeded the threshold $\mathrm{PL}(\hat{\theta}_i) + \chi^2_{1,0.95}$, with $\chi^2_{1,0.95} = 3.84$, on both sides of $\hat{\theta}_i$ within the bounds. The parameter values at which the profile stays below this threshold form the 95% profile-likelihood interval in Table 8.

The normalised sensitivity matrix has full rank (3/3), with singular values 3.35×10^4, 284.9 and 16.03 and condition number 2.09×10^3. No pair of parameters has $|\rho_{ij}| > 0.95$; the correlations are $\rho(\beta_{hl}, \beta_r) = -0.947$, $\rho(\beta_{hl}, \kappa) = -0.596$ and $\rho(\beta_r, \kappa) = 0.812$. The strong negative correlation between β_{hl} and β_r shows that a larger human infection rate can be partly compensated by a smaller rodent infection rate.

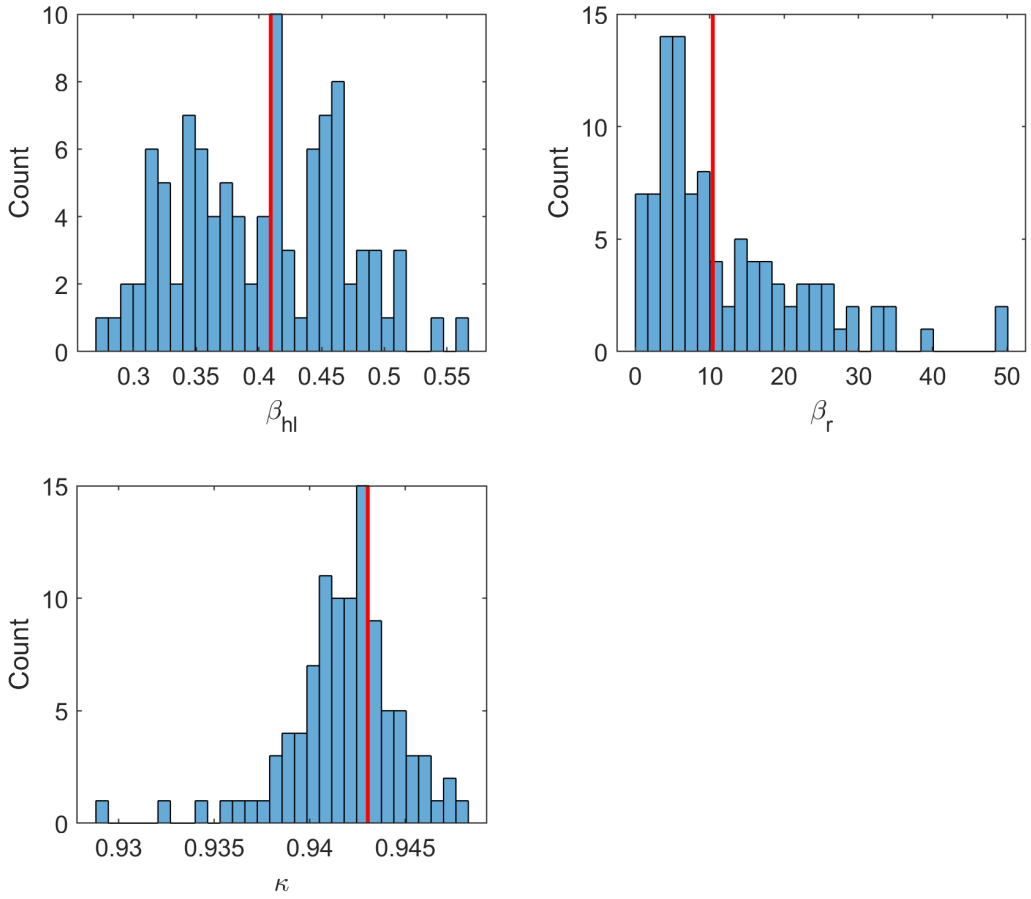


Figure 4. Bootstrap distributions ($B = 100$) of the estimated parameters β_{hl}, β_r and κ of the Lassa fever sub-model. The red lines mark the least-squares estimates.

The profile likelihoods are shown in Figure 5. The profiles of β_{hl} and κ have a clear minimum at the estimate and rise well above the threshold on both sides, so both parameters are practically identifiable. The profile of β_r has a shallow minimum at $\hat{\beta}_r = 10.4$ per week but stays below the threshold over the whole interval $[0, 50]$: the difference between the largest and smallest profile values is only about 3.4, less than $\chi^2_{1,0.95} = 3.84$. Thus, β_r is not practically identifiable from the human case data alone. This is expected, since the 15 cumulative counts of confirmed human cases carry almost no information on infection in the rodent population. The estimate of β_r, and model outputs that depend strongly on it (in particular the dynamics of the rodent compartments), should therefore be interpreted with caution; data on rodent infection prevalence would be needed to determine it. The estimates of β_{hl} and κ, which govern the fitted human epidemic curve, are well determined. Structural identifiability of the full model was not analysed and is left for future work.

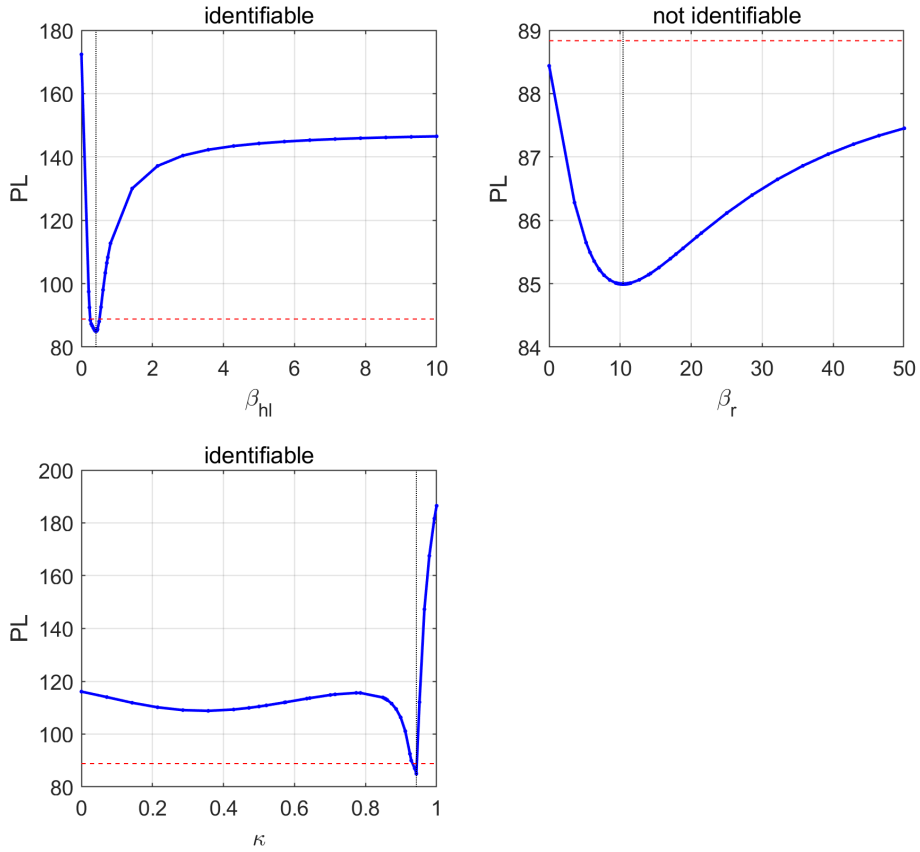


Figure 5. Profile likelihoods of β_{hl}, β_r and κ for the Lassa fever sub-model (blue), with the 95% threshold $\mathrm{PL}(\hat{\theta}_i) + 3.84$ (red, dashed) and the least-squares estimate (dotted).

5.8. Dengue Sub-Model

The dengue sub-model (7) can be fitted and analysed for parameter estimation in exactly the same way as the Lassa fever sub-model. NCDC also reports weekly confirmed dengue cases in Nigeria for the same 16 epidemiological weeks [45]. These data are given in Table 9 so that readers can carry out the analysis. All 16 weeks were reported, so the corresponding objective function uses all $N = 16$ cumulative values, from 21 in week 52 of 2023 to 227 in week 15 of 2024. The cumulative number of symptomatic cases is generated by

$$\frac{dC}{dt} = (1-\kappa)\,\sigma E_d(t), \qquad C(t_0) = 21, \tag{95}$$

which is the flow into I_d in (7). The initial conditions are

$$\begin{aligned} &S_u(0) = 11978, \quad S_e(0) = 102, \quad E_d(0) = 103, \quad I_d(0) = 21, \\ &R(0) = 22, \quad S_v(0) = 500, \quad I_v(0) = 27. \end{aligned} \tag{96}$$

The analogous parameters $\boldsymbol{\theta} = (\beta_{hd}, \beta_v, \kappa)$ are then estimated by minimising the SSE (92) over $\mathcal{J} = \{0, 1, \ldots, 15\}$, with the remaining dengue parameters fixed. The same algorithm, convergence criteria, goodness-of-fit measures, bootstrap and identifiability analysis apply without change.

Table 9. Weekly NCDC dengue data for Nigeria (epidemiological week 52 of 2023 to week 15 of 2024) for fitting the dengue sub-model; $t_j = j$ weeks.

j	Epi-Week	New Confirmed Cases	Cumulative Confirmed Cases, $\tilde{y}_j$
0	52/2023	21	21
1	01/2024	17	38
2	02/2024	10	48
3	03/2024	16	64
4	04/2024	9	73
5	05/2024	12	85
6	06/2024	17	102
7	07/2024	22	124
8	08/2024	18	142
9	09/2024	15	157
10	10/2024	13	170
11	11/2024	16	186
12	12/2024	19	205
13	13/2024	10	215
14	14/2024	5	220
15	15/2024	7	227

6. Sensitivity Analysis

Sensitivity analysis identifies the parameters to which the reproduction number is most responsive, and therefore indicates where intervention effort is best directed. We compute the normalised forward sensitivity index of the control reproduction number $\mathcal{R}_c$ with respect to each parameter ρ, defined by

$$\Upsilon_\rho^{\mathcal{R}_c} = \frac{\partial \mathcal{R}_c}{\partial \rho} \cdot \frac{\rho}{\mathcal{R}_c} = \frac{\partial \ln \mathcal{R}_c}{\partial \ln \rho}. \tag{97}$$

The sign of $\Upsilon_\rho^{\mathcal{R}_c}$ indicates the direction of the effect: a positive index means that an increase in ρ increases $\mathcal{R}_c$, whereas a negative index means that an increase in ρ reduces $\mathcal{R}_c$. The magnitude indicates the relative strength of the effect, with $|\Upsilon_\rho^{\mathcal{R}_c}| = 1$ corresponding to a proportional change.

The indices were computed analytically by differentiating the closed-form expressions for $\mathcal{R}_c^d$ and $\mathcal{R}_c^l$ given in Sections 3 and 4.1 with respect to each parameter, rather than by finite differences, and then evaluating the resulting expressions at the parameter values in Table 7. This avoids numerical error in the signs. Since $\mathcal{R}_c = \max\{\mathcal{R}_c^d, \mathcal{R}_c^l\}$, the index of a parameter equals the index computed from whichever sub-model attains the maximum; parameters that appear only in the other sub-model have zero index at the fitted parameter values. Parameters whose indices are smaller than 10^{-2} in absolute value are not listed in Table 5, because their influence on $\mathcal{R}_c$ is negligible at the fitted values.

The largest positive index is that of the transmission rates β_{hd} and β_v, each with index $+0.50$, reflecting the square-root dependence of $\mathcal{R}_c^d$ on their product. The largest negative index is that of κ, the proportion of exposed individuals who recover without becoming infectious; its magnitude exceeds one because κ is close to unity at the fitted values, so that a small proportional increase in κ produces a large proportional reduction in the remaining infectious fraction $1 - \kappa$. The vector mortality rate μ_v has index -0.50, confirming that reducing mosquito lifespan reduces transmission. The treatment rate π and the dengue-induced death rate d_d both have negative indices, since both shorten the infectious period. The education rate ϵ has a small negative index, indicating that education reduces $\mathcal{R}_c$ but that its effect at the fitted parameter values is modest.

The index of the human mortality rate μ_h deserves separate comment because its sign is not determined by the model structure alone. In $\mathcal{R}_c^d$, μ_h appears in the numerator through

the factor $(\mu_h + \phi_1\epsilon)$ and in the denominator through $k_1 = \sigma + \mu_h$, through $k_2 = \pi + \mu_h + d_d$ and through $(\epsilon + \mu_h)$. Its elasticity is therefore

$$\Upsilon^{\mathcal{R}_c^d}_{\mu_h} = \frac{1}{2}\left[\frac{\mu_h}{\mu_h + \phi_1\epsilon} - \frac{\mu_h}{\sigma + \mu_h} - \frac{\mu_h}{\pi + \mu_h + d_d} - \frac{\mu_h}{\epsilon + \mu_h}\right]. \tag{98}$$

At the fitted parameter values, the first term dominates because σ, π and ϵ are each much larger than μ_h, so that the three negative terms are small. The resulting index is small and positive, indicating that an increase in human mortality slightly increases $\mathcal{R}_c^d$: the rise in the infectious fraction of exposed individuals outweighs the shortening of the infectious period. This effect is weak and should not be interpreted as a policy recommendation.

Taken together, the indices indicate that interventions which reduce the contact rates β_{hd} and β_v, shorten the infectious period through treatment, or increase vector mortality have the greatest leverage on $\mathcal{R}_c$ at the fitted parameter values. Education acts in the same direction but with a smaller effect, and the effect of changes in human mortality is negligible.

7. Numerical Simulation and Discussion

This section presents numerical simulations of the state variables of model (4), using the parameter values in Tables 5 and 8. The simulations show how the state variables respond to changes in key control parameters, and how the compartments behave over the 16-week period covered by the data.

7.1. Numerical Illustration of the Dynamic Model

In this subsection the influence of the key control parameters on each infected compartment of the dengue, Lassa fever and co-infection sub-models is examined. In each figure one parameter is varied while the remaining parameters are held at the fitted values in Tables 5 and 8.

7.1.1. Effect of the Education Rate

Figures 6–12 show the effect of the education campaign on the educated susceptible class S_e and on the exposed, infectious, co-infected and treated classes $E_d, I_d, E_l, I_l, I_{dl}$ and T_{dl} respectively. Figures 7 and 9 show that the exposed dengue and Lassa fever classes peak at an intermediate time when there is no education campaign, and decline more rapidly as the education rate increases, because educated individuals are exposed at the reduced rates $\phi_1\lambda_d$ and $\phi_2\lambda_l$ rather than at the full rates λ_d and λ_l. Figure 6 shows the corresponding rise in the educated susceptible class S_e as education increases: the larger the education rate, the more rapidly individuals move from S_u to S_e, and the smaller the pool of susceptibles exposed at the full force of infection. The reduction in the exposed classes is transmitted to the infectious and co-infected classes in Figures 8–11, all of which decline as education increases. In contrast, treated class increases as the education increases.

The decline in the co-infected class I_{dl} in Figure 11 is slower than the decline in the singly infected classes, because co-infection requires exposure to both pathogens: reducing exposure to one disease alone does not prevent co-infection, and both forces of infection must be reduced before the co-infected classes fall substantially. It should be borne in mind that ϵ is a single rate summarising a complex behavioural process, and that the curves in Figures 6–12 therefore show the consequences of different net rates of transition rather than the effect of any specific campaign design.

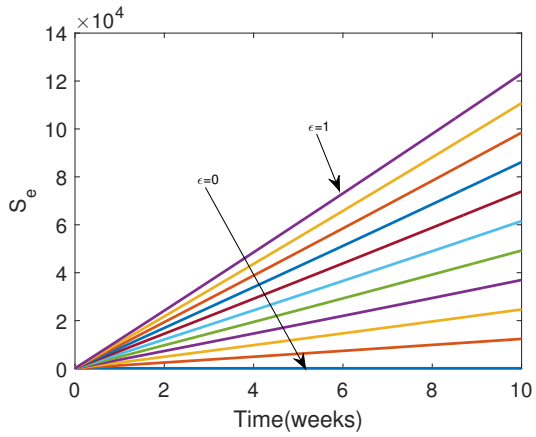


Figure 6. Figure revealing the influence of the Education rate of uneducated susceptible humans with different values of the parameter ϵ on educated susceptible individual, this demonstrates that if the population are being educated about the outbreak of dengue and Lassa fever it will immediately decrease the transmission rate.

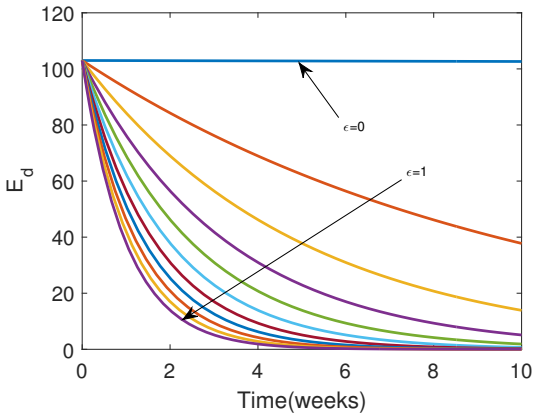


Figure 7. Figure reveals the influence of the education rate of uneducated exposed humans with different values of the parameter ϵ on educated susceptible individuals, demonstrating that educating the exposed individuals about the outbreak of fever will reduce exaltation to dengue hemorrhagic fever.

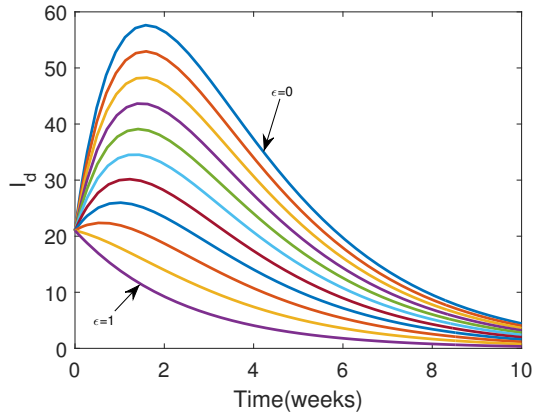


Figure 8. Figure revealing the influence of the Education rate of uneducated susceptible humans with different values of parameter ϵ on Infectious Dengue individuals. It is easy to deduce that educating the uneducated about the outbreak of dengue fever helps in controlling the population of Infectious Dengue fever.

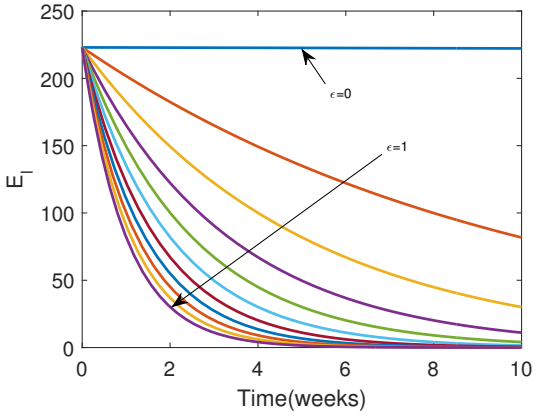


Figure 9. Figure revealing the influence of the Education rate of uneducated susceptible humans with different values of parameter ϵ on Exposed Lassa individuals.It is easy to deduce that as the intensity of education on the Lassa fever outbreak increased Lassa fever infections gradually being controlled in the population of Exposed individuals.

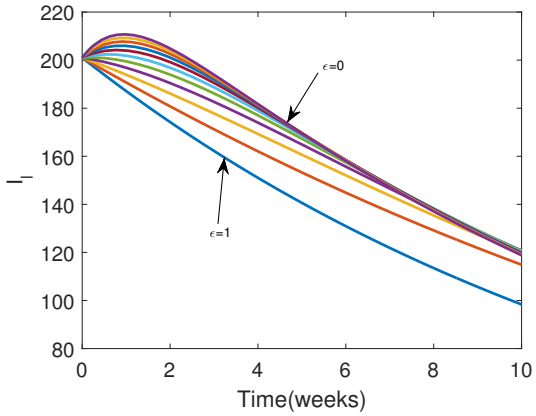


Figure 10. Figure revealing the influence of the Education rate of uneducated susceptible humans with different values of parameter ϵ on Infectious Lassa individuals. It is also easy to deduce that educating the uneducated about Lassa fever helps in controlling the population of Infectious Lassa fever.

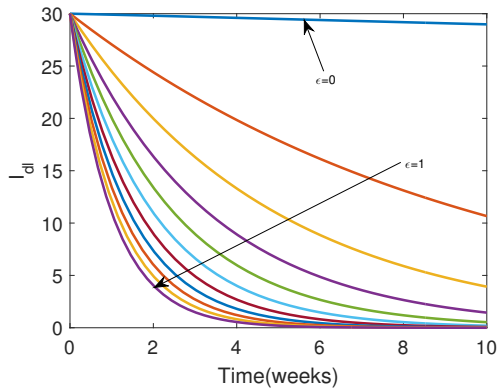


Figure 11. Figure revealing the influence of the Education rate of uneducated susceptible humans with different values of parameter ϵ on individuals co-infected with Lassa and Dengue. It is also easy to deduce that educating the uneducated about Lassa and Dengue fever helps in controlling the population of those that co-infected.

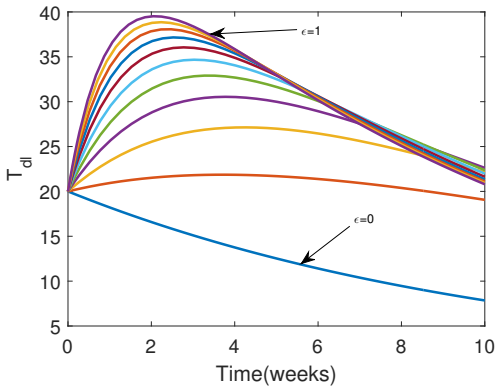


Figure 12. Figure revealing the influence of the Education rate of individuals co-infected with Lassa and Dengue under treatment with different values of parameter ϵ which reveals that even under treatment such individual if properly informed about the outbreak of the disease it controls the spread of the infection.

7.1.2. Effect of the Lassa Fever Treatment Rate

Figures 13 and 14 show the effect of the Lassa fever treatment rate η on the infectious Lassa fever class I_l and on the recovered class R respectively. As η increases, the average time an infectious individual spends in I_l before treatment shortens, so I_l declines more rapidly and to a lower level, while R rises correspondingly. The curves in the two figures are mirror images of one another, because treatment transfers individuals from I_l to R rather than removing them from the population. The effect of η is monotone and develops within the first few weeks, which is consistent with its elasticity index in Table 10: an increase in the treatment rate reduces $\mathcal{R}_c$.

Table 10. Normalised forward sensitivity indices of $\mathcal{R}_c$ with respect to selected parameters, evaluated at the fitted values in Table 7. A positive index indicates that the parameter increases $\mathcal{R}_c$; a negative index indicates that it reduces $\mathcal{R}_c$.

Parameter	Index	Parameter	Index
β_{hd}	+0.50	β_v	+0.50
μ_v	−0.50	ϕ_1	+0.43
π	−0.49	κ	−2.37
d_d	−0.24	σ	+0.01
ϵ	−0.06	μ_h	+0.02

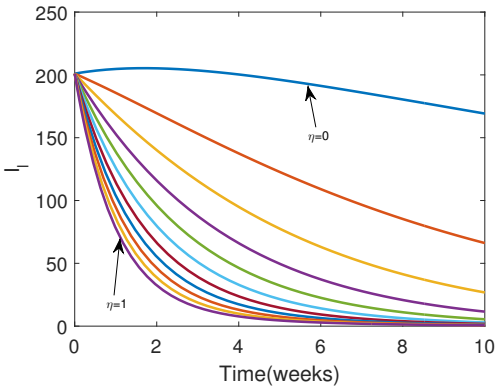


Figure 13. Effect of the Lassa fever treatment rate η on the infectious Lassa fever class I_l. The curves correspond to increasing values of η, with the other parameters held at the base values.

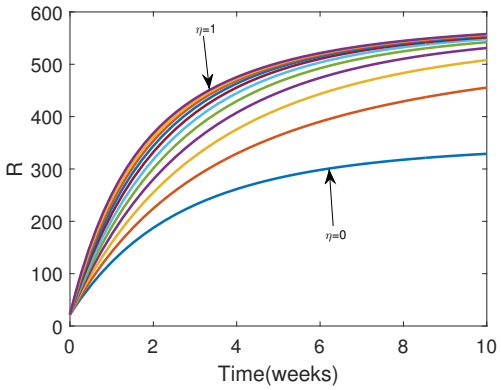


Figure 14. Effect of the Lassa fever treatment rate η on the recovered class R, for the same values of η as in Figure 13. The rise in R mirrors the decline in I_l, since treatment transfers individuals from the infectious to the recovered class.

7.1.3. Effect of the Dengue Treatment Rate

Figures 15–21 show the effect of the dengue treatment rate π on the exposed, infectious, co-infected, treated and recovered classes of both diseases. Figure 16 shows the expected effect: as π increases, the infectious dengue class I_d declines more rapidly, because treatment shortens the average time spent in the infectious state, and Figure 21 shows the corresponding rise in the recovered class R. Figures 15 and 17 show almost coincident curves for the exposed classes E_d and E_l, because π does not enter the equations for the exposed classes: treatment acts on infectious individuals, not on those who have merely been exposed. Any small differences visible in these two figures arise indirectly through the co-infection terms rather than through a direct effect of π on exposure.

Figures 18–20 show the effect of π on the Lassa fever and co-infection compartments, and the pattern is different. The Lassa fever infectious class I_l in Figure 18 is almost unchanged as π increases, because π acts only on the dengue-infected class. The co-infected class I_{dl} in Figure 19 declines slowly, because fewer dengue-infected individuals are available to become co-infected, and the treated co-infected class T_{dl} in Figure 20 declines more slowly still, since T_{dl} is fed by I_{dl} and therefore responds with a further delay. The chain of effects is $\pi \rightarrow I_d \rightarrow I_{dl} \rightarrow T_{dl}$, and each link attenuates the effect of the previous one. This is why treating dengue alone has little influence on co-infection, and why concurrent treatment of both infections is required to reduce the co-infected population substantially.

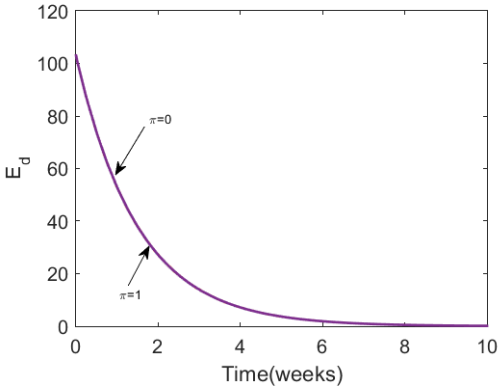


Figure 15. Figure revealing the influence of the Treatment rate of infectious dengue with different values of parameter π on Exposed Dengue individuals, here it indicate that individuals exposed to dengue fever does not need treatment rather they need to be educated on how to control vectors.

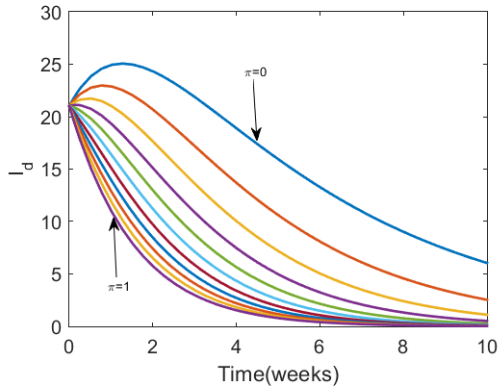


Figure 16. Figure revealing the influence of the Treatment rate of infectious dengue with different values of parameter π on infectious dengue individuals, here the treatment has a significant influence on the infectious dengue individuals, if the magnitude of the treatment it significantly reduces the number of infected people with time.

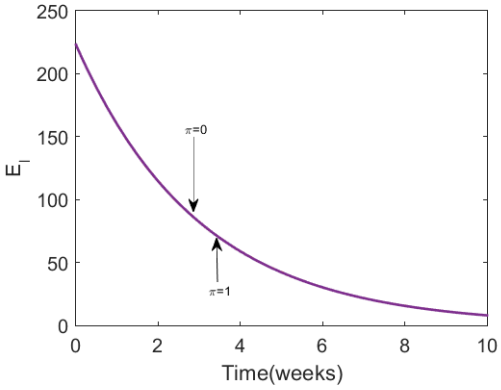


Figure 17. Figure revealing the influence of the Treatment rate of infectious dengue fever with different values of parameter π on Exposed Lassa individuals, which reveals that the treatment rate of infectious dengue fever has no impact on exposed Lassa fever individuals in society.

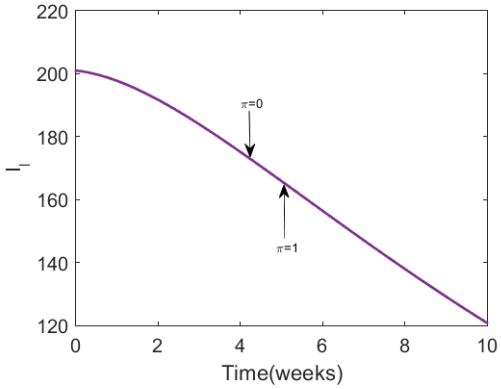


Figure 18. Effect of the dengue treatment rate π on the infectious Lassa fever population I_l. The curves correspond to $\pi \in \{0, 0.2, 0.4, 0.6, 0.8, 1.0\}$ week^{-1}. Since π acts only on the dengue-infected class I_d, treating dengue fever has no direct effect on Lassa fever transmission, and the curves are therefore almost coincident.

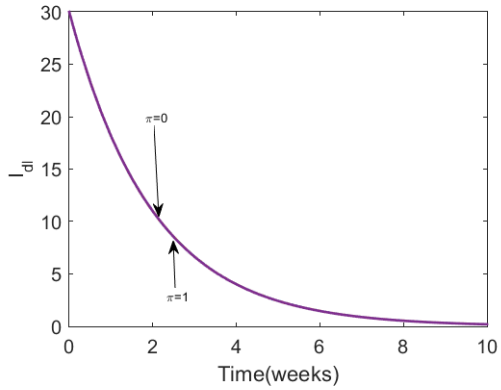


Figure 19. Effect of the dengue treatment rate π on the co-infected population I_{dl}. The curves correspond to $\pi \in \{0, 0.2, 0.4, 0.6, 0.8, 1.0\}$ week^{-1}. The effect is indirect: increasing π reduces the number of dengue-infected individuals I_d available to become co-infected, and therefore lowers I_{dl} with a delay. The reduction is small because co-infection requires simultaneous exposure to both pathogens.

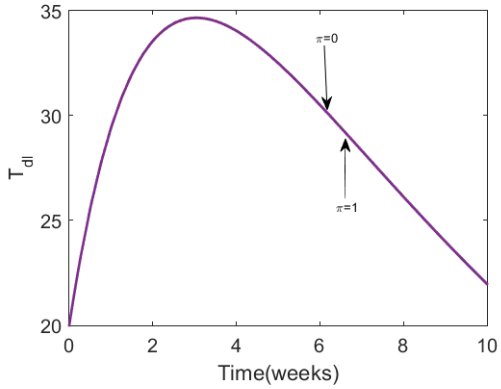


Figure 20. Effect of the dengue treatment rate π on the co-infected population under treatment T_{dl}. The curves correspond to $\pi \in \{0, 0.2, 0.4, 0.6, 0.8, 1.0\}$ week^{-1}. The effect is indirect and operates through the chain $\pi \to I_d \to I_{dl} \to T_{dl}$, so that T_{dl} declines slowly as π increases. Treating only one of the two infections is not sufficient to clear co-infection; concurrent treatment of both is required.

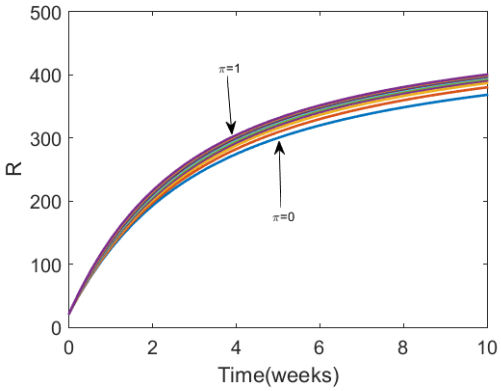


Figure 21. Figure revealing the influence of the Treatment rate of infectious dengue fever with different values of parameter π on Recovered individuals, this reveals that if the treatment of the infectious dengue individuals increases the recovered individual increases in number.

7.1.4. Contour and Surface Plots of the Reproduction Number

Figures 22–27 present contour and surface plots of the dengue control reproduction number $\mathcal{R}_c^d$ as a function of pairs of parameters. In each pair of figures the contour plot and the surface plot show the same information in two forms: the contour plot is easier for reading off the value of $\mathcal{R}_c^d$ at a given combination of parameters, and the surface plot makes the overall shape of the dependence visible.

Figures 22 and 25 show $\mathcal{R}_c^d$ as a function of the education rate ϵ and the proportion κ of exposed individuals who recover without becoming infectious. The reproduction number is highest when both ϵ and κ are small, and declines as either increases. The contours are approximately straight and slope upwards from left to right, which indicates that the two parameters trade off against one another: a higher proportion of individuals recovering without becoming infectious can offset a lower education rate, and vice versa, while leaving $\mathcal{R}_c^d$ unchanged. The steepness of the contours is greater in the direction of κ than in the direction of ϵ, consistent with the elasticity indices in Table 10, where κ has magnitude 2.37 and ϵ has magnitude 0.06.

Figures 23 and 26 show $\mathcal{R}_c^d$ as a function of the two transmission rates β_{hd} and β_v. The reproduction number increases with both, and the contours curve so that the highest values occur when both transmission rates are large. This is the expected consequence of the square-root dependence of $\mathcal{R}_c^d$ on the product $\beta_{hd}\beta_v$: doubling either rate multiplies $\mathcal{R}_c^d$ by $\sqrt{2}$, which is why the contours are convex rather than straight.

Figures 24 and 27 show $\mathcal{R}_c^d$ as a function of the human and vector mortality rates μ_h and μ_v. The reproduction number decreases with both, but the dependence on μ_v is far stronger than the dependence on μ_h: the contours are almost horizontal, so that increasing μ_v over the range shown reduces $\mathcal{R}_c^d$ substantially, whereas increasing μ_h over the same range changes it very little. This asymmetry is consistent with the elasticity indices of -0.50 for μ_v and $+0.02$ for μ_h, and it indicates that vector control, which raises μ_v, is a far more effective lever on $\mathcal{R}_c^d$ than any intervention that acts through human mortality.

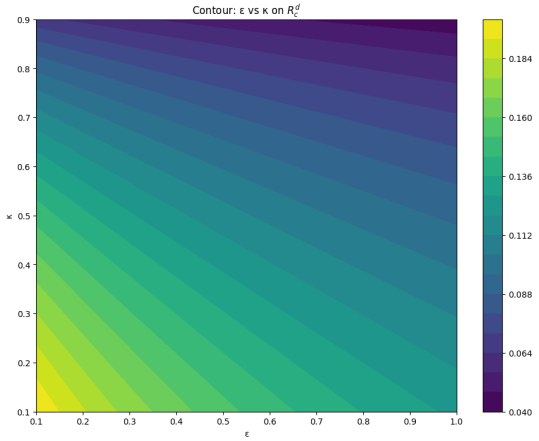


Figure 22. Figure revealing the influence of the Education rate of uneducated susceptible humans versus the proportion of E_d to R and E_l to R on $\mathcal{R}_c^d$.

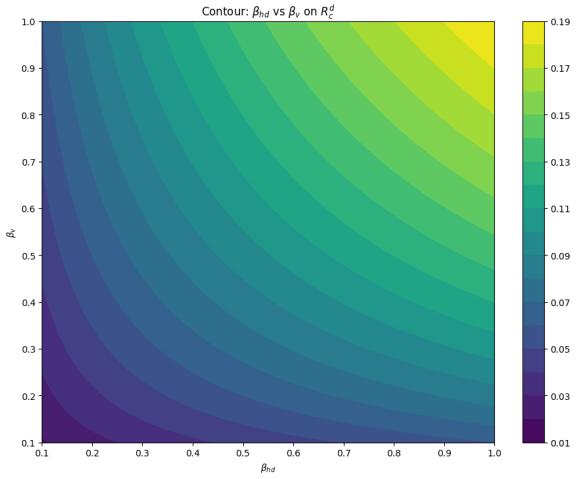


Figure 23. Figure revealing the influence of the β_{hd} versus β_v on $\mathcal{R}_c^d$.

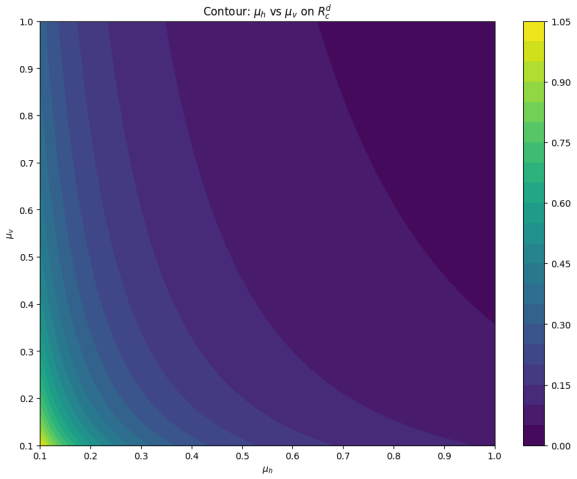


Figure 24. Figure revealing the influence of the μ_h versus μ_v on $\mathcal{R}_c^d$.

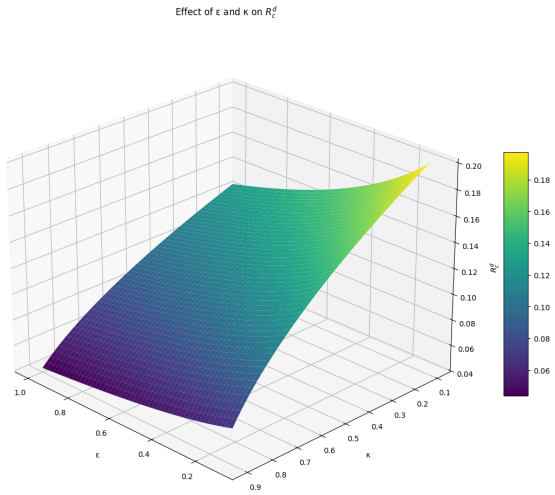


Figure 25. Figure revealing the influence of the Education rate of uneducated susceptible humans versus the proportion of E_d to R and E_l to R on $\mathcal{R}_c^d$.

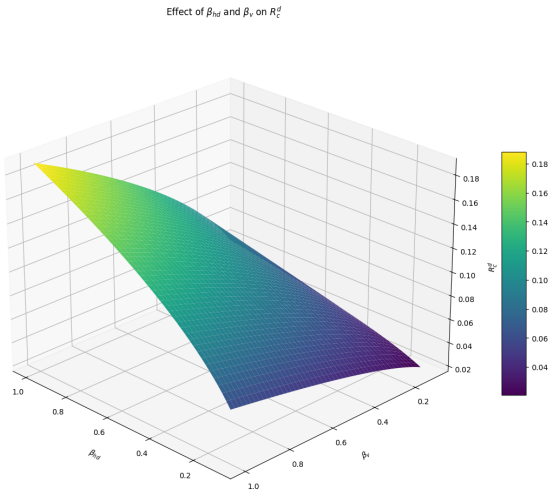


Figure 26. Figure revealing the influence of the β_{hd} and β_v on $\mathcal{R}_c^d$.

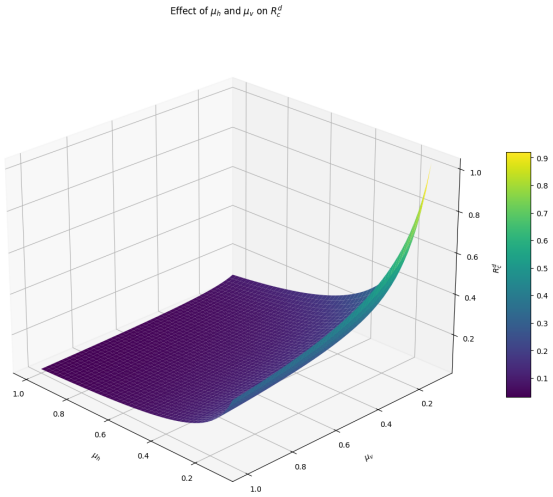


Figure 27. Figure revealing the influence of the μ_h and μ_v on $\mathcal{R}_c^d$.

8. Conclusions

In this paper we developed and analysed a deterministic compartmental model for the co-infection dynamics of dengue and Lassa fever, with explicit representation of educated and uneducated susceptible individuals, of the mosquito and rodent vectors, and of the clinical management of co-infected cases.

The model is epidemiologically well posed: solutions remain positive and bounded for all positive initial data, and the disease-free equilibrium exists for all parameter values. The control reproduction number $\mathcal{R}_c$ governs the local and global stability of the disease-free equilibrium: when $\mathcal{R}_c < 1$ it is globally asymptotically stable. When $\mathcal{R}_c > 1$, the endemic equilibria of the two sub-models are globally asymptotically stable under the additional condition $\psi = \kappa = 0$. These stability results concern the reduced dengue and Lassa fever sub-systems; global stability of an endemic equilibrium of the full co-infection model is not established here and is left for future work.

The sensitivity analysis identified κ, the proportion of exposed individuals who recover without becoming infectious, as the parameter with the largest elasticity index in absolute value, -2.37, because κ is close to unity at the fitted values. The transmission rates β_{hd} and β_v follow, each with index $+0.50$, then the vector mortality rate μ_v with index -0.50, and the

dengue treatment rate π with index -0.49. The education rate ϵ has a smaller index, -0.06, indicating that education reduces $\mathcal{R}_c$ but with less leverage than direct vector control or treatment at the fitted parameter values.

The numerical simulations are consistent with these analytical results. Increasing the education rate lowers the incidence of both diseases by moving individuals into the educated susceptible class, where exposure occurs at the reduced rates $\phi_1\lambda_d$ and $\phi_2\lambda_l$ (Figures 6–12). Increasing the Lassa fever treatment rate η reduces the infectious Lassa fever class and raises the recovered class (Figures 13 and 14). Increasing the dengue treatment rate π reduces the infectious dengue class and, indirectly and more slowly, the co-infected and treated co-infected classes (Figures 18–20). Treating one disease alone has little effect on co-infection, which supports the conclusion that concurrent treatment of both infections is necessary.

The study has limitations. The model was fitted to 16 weekly observations for each disease, which limits the number of parameters that can be estimated reliably and means that the fitted values should be interpreted as model-derived quantities rather than as definitive epidemiological estimates. The sub-models were fitted separately rather than the full co-infection model, so the fitted parameters reproduce the single-disease dynamics and the co-infection dynamics are a prediction of the model rather than a calibrated output. The model assumes homogeneous mixing within the educated and uneducated classes, does not distinguish dengue serotypes, and does not include human-to-human transmission of Lassa fever. These simplifications were made to keep the model tractable, but they mean that the quantitative predictions should be treated with caution.

Future work should extend the model in four directions: to include serotype structure and antibody-dependent enhancement for dengue; to incorporate spatial heterogeneity and seasonality, both of which are known to affect dengue and Lassa fever transmission in West Africa; a to fit the full co-infection model to longer data series using Bayesian estimation with informative priors, which would allow parameter uncertainty to be quantified and would improve identifiability. A fourth direction is to replace the integer-order derivative by a fractional operator, as has been done for other biomedical models [25,27,28]; this would allow the memory trace of past incidence to enter the current dynamics, which is of interest for a disease with the long and variable incubation period of Lassa fever.

Taken together, the results indicate that reducing human–vector contact, increasing vector mortality, and treating both infections concurrently are the interventions with the greatest leverage on $\mathcal{R}_c$ in this setting. Education acts in the same direction but with a smaller effect at the fitted parameter values. These findings provide a quantitative basis for prioritising interventions in regions where dengue and Lassa fever co-circulate.

Recommendation and Future Work

This work can be extended by examining the following: Environmental considerations include the climate, terrain, and cleanliness of the community in the studied location. Individual immune system differences; some are believed to have a strong immune system that is resistant to infection, while others are believed to have a weak immune system, making them easily infected. Such discrepancies should be taken into account. The transmission of diseases such as dengue and Lassa fever can be influenced by demographic factors such as family history, population density, and family relationships.

Author Contributions: Conceptualization, K.B.; methodology, K.B., F.A.A., M.O.A.; software, M.O.A., S.Q., A.S. and J.A.; validation, F.A.A., M.O.A., J.A. and C.K.; formal analysis, J.A., S.Q. and A.S.; investigation, F.A.A., M.O.A., J.A., and C.K.; resources, C.K., I.A. and J.A.; data curation, J.A., S.Q., and A.S.; writing-original draft preparation, K.B.; writing-review and editing, F.A.A., M.O.A., J.A.,

S.A., and R.M.N.; visualization, M.O.A., J.A., S.Q., and A.S.; supervision, F.A.A., M.O.A., and C.K.; project administration, K.B., F.A.A., M.O.A., and C.K.; funding acquisition, C.K. All authors have read and agreed to the published version of the manuscript.

Funding: This research budget was allocated by National Science, Research and Innovation Fund (NSRF) and King Mongkut's University of Technology North Bangkok with Contract no. KMUTNB-67-KNOW-28.

Data Availability Statement: All Data used for this research can be found in the article.

Acknowledgments: The authors sincerely appreciate TETFund for the scholarship award and the management of Federal University Lokoja. REF: TETF/ES/UNI/KOGI/TSAS/2022.

Conflicts of Interest: The authors declare no conflict of interest.

References

1. Abdulhamid, A.; Hussaini, N.; Musa, S.S.; He, D. Mathematical analysis of Lassa fever epidemic with effects of environmental transmission. *Results Phys.* **2022**, *35*, 105335. [CrossRef]
2. Abidemi, A.; Abd Aziz, M.I.; Ahmad, R. Vaccination and vector control effect on dengue virus transmission dynamics: Modelling and simulation. *Chaos Solitons Fractals* **2020**, *133*, 109648. [CrossRef]
3. Collins, O.C.; Duffy, K.J. Using Data of a Lassa Fever Epidemic in Nigeria: A Mathematical Model Is Shown to Capture the Dynamics and Point to Possible Control Methods. *Mathematics* **2023**, *11*, 1181. [CrossRef]
4. Hemorrhagic Fevers. (n.d.). Leeds, Grenville and Lanark District Health Unit. Available online: https://healthunit.org/for-professionals/health-care-dental/communicable-disease-resources/reportable-disease-toolkit/hemorrhagic-fevers/ (accessed on 12 March 2022).
5. Ojo, M.M.; Goufo, E.F.D. Modeling, analyzing and simulating the dynamics of Lassa fever in Nigeria. *J. Egypt. Math. Soc.* **2022**, *30*, 1. [CrossRef]
6. Nigeria Centers for Disease Control and Prevention. Signs and Symptoms Lassa Fever. Available online: https://www.cdc.gov/lassa-fever/about/index.html (accessed on 6 March 2019).
7. Ramzan, Y.; Awan, A.U.; Ozair, M.; Hussain, T.; Mahat, R. Innovative strategies for Lassa fever epidemic control: A groundbreaking study. *AIMS Math.* **2023**, *8*, 30790–30812. [CrossRef]
8. Bitrus, K.; Abdullah, F.A.; Adewole, M.O.; Andrawus, J.; Qureshi, S.; Soomro, A.; Yusuf, A. Uncovering the influence of public awareness on dengue population dynamics: A mathematical model approach. *Bol. Soc. Mat. Mex.* **2025**, *31*, 86. [CrossRef]
9. Adeleke, M.A.; Sam-Wobo, S.O.; Garza-Hernandez, J.A.; Oluwole, A.S.; Mafiana, C.F.; Reyes-Villanueva, F.; Rodriguez-Perez, M.A. Twenty-Three Years after the First Record of Aedes albopictus in Nigeria: Its Current Distribution and Potential Epidemiological Implications. *Afr. Entomol.* **2015**, *23*, 348–355. [CrossRef]
10. Aguiar, M.; Anam, V.; Blyuss, K.B.; Estadilla, C.D.S.; Guerrero, B.V.; Knopoff, D.; Kooi, B.W.; Srivastav, A.K.; Steindorf, V.; Stollenwerk, N. Mathematical models for dengue fever epidemiology: A 10-year systematic review. *Phys. Life Rev.* **2022**, *40*, 65–92. [CrossRef] [PubMed]
11. Bello, O.; Aminu, M.; Jatau, E. Seroprevalence of IgM Antibodies to Dengue Fever Virus among Patients Presenting with Symptoms of Fever in Some Hospitals in Kaduna State, Nigeria. *Int. J. Sci. Res. (IJSR)* **2016**, *5*, 1255–1259. [CrossRef]
12. Chanprasopchai, P.; Tang, I.M.; Pongsumpun, P. SIR Model for Dengue Disease with Effect of Dengue Vaccination. *Comput. Math. Methods Med.* **2018**, *2018*, e9861572. [CrossRef] [PubMed]
13. Morens, D.M. Dengue Fever and Dengue Hemorrhagic Fever. *Pediatr. Infect. Dis. J.* **2009**, *28*, 635–636. [CrossRef] [PubMed]
14. Mekonen, K.G.; Balcha, S.F.; Obsu, L.L.; Hassen, A. Mathematical Modeling and Analysis of TB and COVID-19 Coinfection. *J. Appl. Math.* **2022**, *2022*, 2449710. [CrossRef]
15. Adewole, M.O.; Abdullah, F.A.; ALI. Dynamics of leptospirosis in human and rodent population: A multiscale modeling approach. *J. Biol. Syst.* **2024**, *32*, 605–641. [CrossRef]
16. Andrawus, J.; Muhammad, A.I.; Denue, B.A.; Abdul, H.; Yusuf, A.; Salahshour, S. Unraveling the importance of early awareness strategy on the dynamics of drug addiction using mathematical modeling approach. *Chaos An. Interdiscip. J. Nonlinear Sci.* **2024**, *34*, 083112. [CrossRef] [PubMed]
17. Andrawus, J.; Yusuf, A.; Mustapha, U.T.; Alshomrani, A.S.; Baleanu, D. Unraveling the dynamics of Ebola virus with contact tracing as control strategy. *Fractals* **2023**, *31*, 2340. [CrossRef]
18. Kelemu Mengistu, A.; Witbooi, P.J. Modeling the Effects of Vaccination and Treatment on Tuberculosis Transmission Dynamics. *J. Appl. Math.* **2019**, *2019*, 1–9. [CrossRef]

19. Lambrechts, L.; Scott, T.W.; Gubler, D.J. Consequences of the Expanding Global Distribution of Aedes albopictus for Dengue Virus Transmission. *PLoS Neglected Trop. Dis.* **2010**, *4*, e646. [CrossRef] [PubMed]
20. Sulayman, F.; Abdullah, F.A. Analysis of a Tuberculosis Infection Model considering the Influence of Saturated Recovery (Treatment). *Complexity* **2021**, e1805651. [CrossRef]
21. Ibrahim, M.A.; Dénes, A. A mathematical model for Lassa fever transmission dynamics in a seasonal environment with a view to the 2017–20 epidemic in Nigeria. *Nonlinear Anal. Real. World Appl.* **2021**, *60*, 103310. [CrossRef]
22. Fagbami, A.H.; Onoja, A.B. Dengue hemorrhagic fever: An emerging disease in Nigeria, West Africa. *J. Infect. Public Health* **2018**, *11*, 757–762. [CrossRef] [PubMed]
23. Lasluisa, D.; Barrios, E.; Vasilieva, O. Optimal Strategies for Dengue Prevention and Control during Daily Commuting between Two Residential Areas. *Processes* **2019**, *7*, 197. [CrossRef]
24. Naphtali, R.S.; Ngwamah, J.S. Phytochemical Screening and Larvicidal Activities of Some Ethnobotanicals from North Eastern Nigeria against Culicine (Diptera: Culicidae) Mosquito. *Int. J. Trop. Dis. Health* **2019**, *37*, 1–9. [CrossRef]
25. Özköse, F. Modeling of psoriasis by considering drug influence: A mathematical approach with memory trace. *Comput. Biol. Med.* **2024**, *168*, 107791. [CrossRef] [PubMed]
26. Weerasuriya, C.K.; Harris, R.C.; McQuaid, C.F.; Bozzani, F.; Ruan, Y.; Li, R.; Li, T.; Rade, K.; Rao, R.; Ginsberg, A.M.; et al. The epidemiologic impact and cost-effectiveness of new tuberculosis vaccines on multidrug-resistant tuberculosis in India and China. *BMC Med.* **2021**, *19*, 60. [CrossRef] [PubMed]
27. Özköse, F.; Yılmaz, S.; Şenel, M.T.; Yavuz, M.; Townley, S.; Doğan Sarıkaya, M. A mathematical modeling of patient-derived lung cancer stem cells with fractional-order derivative. *Phys. Scr.* **2024**, *99*, 115235. [CrossRef]
28. Kaya, E.; Özköse, F.; Şenel, M. Caputo fractional-order model of measles and Reye's syndrome: Insights from UK surveillance data on stability and bifurcation. *Electron. Trans. Numer. Anal.* **2026**, *65*, 441–478. [CrossRef]
29. Fawzy, D.M.; Elsaid, A.; Zahra, W.K.; Arafa, A.A. Qualitative analysis of a Filippov wild-sterile mosquito population model with immigration. *Chaos An. Interdiscip. J. Nonlinear Sci.* **2023**, *33*, 113101. [CrossRef] [PubMed]
30. Fawzy, D.M.; Arafa, A.A.; Elsaid, A.; Zahra, W.K. Mosquito suppression via Filippov incompatible insect technique. *Appl. Math. Comput.* **2024**, *480*, 128908. [CrossRef]
31. Hasan, M.R.; Hobiny, A.; Alshehri, A. Analysis of vector-host SEIR-SEI dengue epidemiological model. *Int. J. Anal. Appl.* **2022**, *20*, 57. [CrossRef]
32. Alharbi, T.D.; Hasan, M.R. Global stability and sensitivity analysis of vector-host dengue mathematical model. *AIMS Math.* **2024**, *9*, 32797–32818. [CrossRef]
33. Diekmann, O.; Heesterbeek, J.A.P.; Metz, J.A.J. On the definition and the computation of the basic reproduction ratio R 0 in models for infectious diseases in heterogeneous populations. *J. Math. Biol.* **1990**, *28*, 365–382. [CrossRef] [PubMed]
34. Van Den Driessche, P.; Watmough, J. Reproduction numbers and sub-threshold endemic equilibria for compartmental models of disease transmission. *Math. Biosci.* **2002**, *180*, 29–48. [CrossRef] [PubMed]
35. Lasalle, J.P. The stability of dynamical systems. In *Proceedings of the Regional Conference Series in Applied Mathematics*; SIAM: Philadelphia, PA, USA, 1976.
36. Nigeria Center for Disease Control and Prevention. An Update of Lassa Fever Outbreak in Nigeria. 2024. Available online: https://ncdc.gov.ng/diseases/sitreps (accessed on 4 October 2025).
37. Patrick, O.N.; Ifeoma, N.V.; Abu, O. Mathematical model for the transmission dynamics of Lassa fever with control. *Sci. J.* **2020**, *15*, 62–68. [CrossRef]
38. Eguda, F.Y.; James, A.; Babuba, S. The Solution of a Mathematical Model for Dengue Fever Transmission Using Differential Transformation Method. *J. Niger. Soc. Phys. Sci.* **2019**, *1*, 82–87. [CrossRef]
39. Ahmad, Y.U.; Mustapha, U.T.; Ado, A.; Abdullahi, I. Evaluating the impact of chemoprevention on malaria transmission dynamics in Jigawa State, Nigeria: A mathematical modeling approach. *Dutse J. Pure Appl. Sci.* **2026**, *12*, 101–117.
40. Branch, M.A.; Coleman, T.F.; Li, Y. A subspace, interior, and conjugate gradient method for large-scale bound-constrained minimization problems. *SIAM J. Sci. Comput.* **1999**, *21*, 1–23. [CrossRef]
41. Coleman, T.F.; Li, Y. An interior trust region approach for nonlinear minimization subject to bounds. *SIAM J. Optim.* **1996**, *6*, 418–445. [CrossRef]
42. Burnham, K.P.; Anderson, D.R. *Model Selection and Multimodel Inference: A Practical Information-Theoretic Approach*, 2nd ed.; Springer: Berlin/Heidelberg, Germany, 2002.
43. Chowell, G. Fitting dynamic models to epidemic outbreaks with quantified uncertainty: A primer for parameter uncertainty, identifiability, and forecasts. *Infect. Dis. Model.* **2017**, *2*, 379–398. [CrossRef] [PubMed]

44. Raue, A.; Kreutz, C.; Maiwald, T.; Bachmann, J.; Schilling, M.; Klingmüller, U.; Timmer, J. Structural and practical identifiability analysis of partially observed dynamical models by exploiting the profile likelihood. *Bioinformatics* **2009**, *25*, 1923–1929. [CrossRef] [PubMed]
45. Nigeria Center for Disease Control and Prevention. An Update of Dengue Fever Outbreak in Nigeria. 2025. Available online: https://ncdc.gov.ng/diseases/a-z (accessed on 20 January 2026).

Disclaimer/Publisher's Note: The statements, opinions and data contained in all publications are solely those of the individual author(s) and contributor(s) and not of MDPI and/or the editor(s). MDPI and/or the editor(s) disclaim responsibility for any injury to people or property resulting from any ideas, methods, instructions or products referred to in the content.